Article

Theory and Practice of Enzyme Bioaffinity Electrodes. Direct Electrochemical Product Detection

Benoi#t Limoges, Damien Marchal, François Mavré, Jean-Michel Savéant, and Bernd Schöllhorn

J. Am. Chem. Soc., **2008**, 130 (23), 7259-7275 • DOI: 10.1021/ja7102845 • Publication Date (Web): 20 May 2008

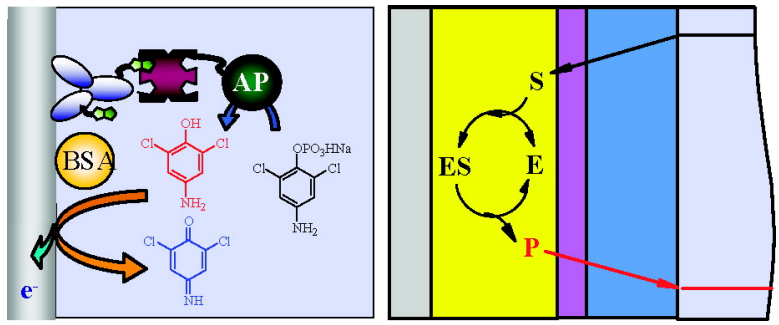

More About This Article

Additional resources and features associated with this article are available within the HTML version:

- Supporting Information
- Links to the 1 articles that cite this article, as of the time of this article download
- Access to high resolution figures
- Links to articles and content related to this article
- Copyright permission to reproduce figures and/or text from this article

View the Full Text HTML

J|A|C|S
ARTICLES

Published on Web 05/20/2008

Theory and Practice of Enzyme Bioaffinity Electrodes. Direct Electrochemical Product Detection

Benoît Limoges,*,† Damien Marchal,† François Mavré,† Jean-Michel Savéant,*,† and Bernd Schöllhorn‡

Laboratoire d'Electrochimie Moléculaire, Université Paris Diderot, UMR CNRS 7591, 2 place Jussieu, 75251 Paris Cedex 05, France, and Département de Chimie, Ecole Normale Supérieure, UMR CNRS 8640-PASTEUR, 24 rue Lhomond, 75231 Paris Cedex 05, France

Received November 22, 2007; E-mail: limoges@univ-paris-diderot.fr; saveant@univ-paris-diderot.fr

Abstract: The use of enzyme labeling techniques to convert biorecognition events into high sensitivity electrochemical signals may follow two different strategies. One, in which the current is the electrocatalytic response of a redox couple serving as cosubstrate to a redox enzyme label and another that consists in the detection of an electrochemically active product of the enzyme label. The theoretical relationships that link, in the latter case, the electrochemical current response to the amount of recognized labeled target analyte are established for steady-state diffusion-convection chronoamperometric regimes. Two governing parameters thus emerge. One measures the Michaelis–Menten competition in the enzyme kinetics. The other characterizes the competition between the enzymatic kinetics and the diffusion of the substrate. The electrochemical response is finally related to the labeled target analyte concentration in solution through the recognition isotherm. The direct electrochemical product detection thus provides a route to the characteristics of the recognition isotherm, which serves as a calibration curve in analytical applications. The establishment of further theoretical relationships allows one to surmise the increase in sensitivity that may be obtained by using cyclic voltammetry instead of steady-state chronoamperometry in standard electrochemical cells or by accumulation of the enzyme–product in cells of small volume/surface ratios. The theoretical predictions are tested with the example of the avidin–biotin recognition process in a system that involves alkaline phosphatase as enzyme label and 4-amino-2,6-dichlorophenyl phosphate as substrate, generating 4-amino-2,6-dichlorophenol as electrochemically active product. The advantages of the dichloro-substitution are discussed. The theoretical analysis is a requisite for a rational and realistic discussion of the analytical performances of the steady-state chronoamperometric and cyclic voltammetric approaches. These are shown to compare favorably with the best heterogeneous bioaffinity assays so far reported.

Introduction

Enzyme-amplified bioaffinity electrodes, based on a receptor–ligand binding, for example, immuno- and DNA-sensors, have attracted considerable attention as biosensors in recent years, and have emerged as viable alternatives to conventional spectrophotometric enzyme affinity assays.[1–4] They can reach low-level detection with a high selectivity in small volumes (not limited, as with optical methods, by the Beer–Lambert law). They are also robust, economical to mass produce, and can be easily miniaturized to circuit board level with low power requirements, being thus good candidates for the development of field-portable analytical instrumentations and integration into multiarrays, microfluidic chips, and other microsensing devices for multianalyte detection. Assays by means of enzyme-amplified bioaffinity electrodes are a particular class of heterogeneous enzyme bioaffinity assays in which the electrode serves both as an immobilization platform and as a detector to reveal, with the help of an enzyme label, the specific bimolecular recognition between the immobilized ligand (e.g., antibody, oligonucleotide, carbohydrate, biotin) and a target receptor (e.g., antigen, DNA fragment, protein, avidin) present in solution. The enzyme label not only effects the transduction of the biomolecular recognition event into an electrochemical signal but also allows its amplification according to the catalytic activity of the enzyme, leading to the possibility of developing highly sensitive affinity sensors. The fact that recognition occurs at the electrode surface entails that the enzymatic reaction takes place in its close vicinity leading to a fast setting up of the electrochemical response. It also opens a route to an array of electrodes for multianalyte analysis, taking advantage of the spatial discrimination of the enzyme-amplified electrochemical response.[5] Enzyme labeling techniques converting a biorecognition event into an electrochemical signal may be applied in two ways. In one of these, the current is the electrocatalytic response of a redox couple serving as cosubstrate to a redox enzyme label (Scheme 1a).[6–11] The other consists in the

† Université Paris Diderot.
‡ Ecole Normale Supérieure.

(1) Díaz-González, M.; González-García, M. B.; Costa-García, A. *Electroanalysis* **2005**, *17*, 1901–18.
(2) Skladal, P. *Electroanalysis* **1997**, *9*, 737–45.
(3) Killard, A. J.; Smyth, M. R. *Anal. Lett.* **2000**, *33*, 1451–65.
(4) Wang, J. *Biosens. Bioelectron* **2006**, *21*, 1887–92.
(5) Wilson, M. S.; Nie, W. *Anal. Chem.* **2006**, *78*, 2507–13.

10.1021/ja7102845 CCC: $40.75

Scheme 1

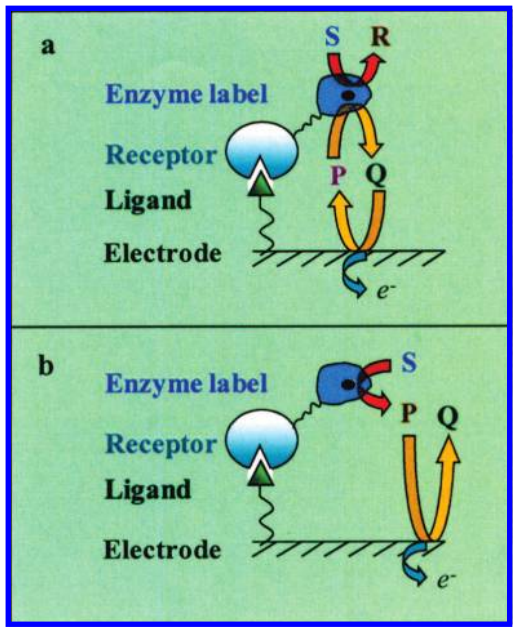

detection of an electrochemically active product of the enzyme label (Scheme 1b).[5,12–41]

Despite the large number of enzyme-amplified bioaffinity electrodes described in the literature, little effort has been made so far to establish rigorously the relationships that link the electrochemical responses to the surface and bulk concentrations of the enzyme-labeled target analyte, which form the necessary basis for determining the recognition binding characteristics as well as for a realistic evaluation of the analytical performances (sensitivity, detection limit, linear dynamic range of the analyte concentration) of such electrodes. The few exceptions to this lack of theoretical analyses have concerned the redox enzyme-labeled systems[42a,b] and not the systems based on the electrochemical detection of the enzyme label product.

The aim of the present two companion papers is to fill this theoretical gap. The first paper is devoted to the various modes of direct electrochemical detection. In the second,[43] we discuss chemical and enzymatic means of amplifying the electrochemical response.

Concerning direct electrochemical detection, we first establish the relationships that link the electrochemical current response to the amount of recognized labeled target analyte for a steady-state diffusion-convection chronoamperometric regime. The electrochemical response is then related to the labeled target analyte concentration in solution through the recognition isotherm, thus offering a way to determine its characteristics and leading to a rational estimation of the analytical performances. The establishment of further theoretical relationships allows the estimation of the increase in sensitivity that may be obtained by using cyclic voltammetry instead of steady-state diffusion-natural convection chronoamperometry in a standard electrochemical cell or by accumulation of the enzyme–product in a system of very low volume/surface ratios.

The theoretical analysis is then illustrated with the avidin–biotin recognition process in a system that involves alkaline phosphatase (AP) as enzyme label and 4-amino-2,6-dichlorophenyl phosphate as substrate, generating 4-amino-2,6-dichlorophenol as the electrochemically active product. More precisely, the system is as depicted in Scheme 2, showing the binding of alkaline phosphatase-conjugated neutravidin (N-AP)[44] to a monolayer of biotinylated immunoglobulin (b-IgG) irreversibly adsorbed on the surface of the electrode,[45] followed by the

(6) Campbell, C. N.; De Lumley-Woodyear, T.; Heller, A. *Fresenius J. Anal. Chem.* **1999**, *364*, 165–9.
(7) Rishpon, J.; Ivnitski, D. *Biosens. Bioelectron.* **1997**, *12*, 195–204.
(8) Caruana, D. J.; Heller, A. *J. Am. Chem. Soc.* **1999**, *121*, 769–74.
(9) Kavanagh, P.; Leech, D. *Anal. Chem.* **2006**, *78*, 2710–6.
(10) Kim, H. H.; Zhang, Y.; Heller, A. *Anal. Chem.* **2004**, *76*, 2411–4.
(11) De Lumley-Woodyear, T.; Campbell, C. N.; Heller, A. *J. Am. Chem. Soc.* **1996**, *118*, 5504–5.
(12) Azek, F.; Grossiord, C.; Joannes, M.; Limoges, B.; Brossier, P. *Anal. Biochem.* **2000**, *284*, 107–13.
(13) Kojima, K.; Hiratsuka, A.; Suzuki, H.; Yano, K.; Ikebukuro, K.; Karube, I. *Anal. Chem.* **2003**, *75*, 1116–22.
(14) Volpe, G.; Fares, G.; delli Quadri, F. ; Draisci, R.; Ferretti, G.; Marchiafava, C.; Moscone, D.; Palleschi, G. *Anal. Chim. Acta* **2006**, *572*, 11–6.
(15) Butler, D.; Guilbault, G. G. *Sens. Actuators, B* **2006**, *B113*, 692–9.
(16) Diaz-Gonzalez, M.; Gonzalez-Garcia, M. B.; Costa-Garcia, A. *Sens. Actuators, B* **2006**, *B113*, 1005–11.
(17) Xu, Y. F.; Velasco-Garcia, M.; Mottram, T. T. *Biosens. Bioelectron.* **2005**, *20*, 2061–70.
(18) Díaz-González, M.; González-García, M. B.; Costa-García, A. *Biosens. Bioelectron* **2005**, *20*, 2035–43.
(19) Wilson, M. S. *Anal. Chem.* **2005**, *77*, 1496–502.
(20) Ammida, N. H. S.; Volpe, G.; Draisci, R.; delli Quadri, F.; Palleschi, L.; Palleschi, G. *Analyst* **2004**, *129*, 15–9.
(21) Vetcha, S.; Wilkins, E.; Yates, T. *Biosens. Bioelectron.* **2002**, *17*, 901–9.
(22) O'Regan, T. M.; O'Riordan, L. J.; Pravda, M.; O'Sullivan, C. K.; Guilbault, G. G. *Anal. Chim. Acta* **2002**, *460*, 141–50.
(23) Pemberton, R. M.; Hart, J. P.; Stoddard, P.; Foulkes, J. A. *Biosens. Bioelectron.* **1999**, *14*, 495–503.
(24) Schreiber, A.; Feldbrugge, R.; Key, G.; Glatz, J. F. C.; Spener, F. *Biosens. Bioelectron.* **1997**, *12*, 1131–7.
(25) Rosen, I.; Rishpon, J. *J. Electroanal. Chem.* **1989**, *258*, 27–39.
(26) Duan, C.; Meyerhoff, M. E. *Anal. Chem.* **1994**, *66*, 1369–77.
(27) Aguilar, Z. P.; Vandaveer, W. R.; Fritsch, I. *Anal. Chem.* **2002**, *74*, 3321–9.
(28) Elsholz, B.; Woerl, R.; Blohm, L.; Albers, J.; Feucht, H.; Grunwald, T.; Juergen, B.; Schweder, T.; Hintsche, R. *Anal. Chem.* **2006**, *78*, 4794–802.
(29) Bagel, O.; Degrand, C.; Limoges, B.; Joannes, M.; Azek, F.; Brossier, P. *Electroanalysis* **2000**, *12*, 1447–52.
(30) Aguilar, Z. P.; Fritsch, I. *Anal. Chem.* **2003**, *75*, 3890–7.
(31) Aguilar, Z. P. *Anal. Chem.* **2006**, *78*, 1122–9.
(32) Carpini, G.; Lucarelli, F.; Marrazza, G.; Mascini, M. *Biosens. Bioelectron.* **2004**, *20*, 167–75.
(33) Hernández-Santos, D.; Diaz-González, M.; Gonzalez-García, M. B.; Costa-García, A. *Anal. Chem.* **2004**, *76*, 6887–93.
(34) Abad-Valle, P.; Fernandez-Abedul, M. T.; Costa-García, A. *Biosens. Bioelectron.* **2005**, *20*, 2251–60.
(35) Liu, D.; Perdue, R. K.; Sun, L.; Crooks, R. M. *Langmuir* **2004**, *20*, 5905–10.
(36) Nebling, E.; Grunwald, T.; Albers, J.; Schaefer, P.; Hintsche, R. *Anal. Chem.* **2004**, *76*, 689–96.
(37) Patolsky, F.; Lichtenstein, A.; Willner, I. *Chem. Eur. J.* **2003**, *9*, 1137–45.
(38) Patolsky, F.; Lichtenstein, A.; Willner, I. *Nat. Biotechnol.* **2001**, *19*, 253–7.
(39) Lucarelli, F.; Marrazza, G.; Mascini, M. *Langmuir* **2006**, *22*, 4305–9.
(40) Fojta, M.; Brazdilova, P.; Cahova, K.; Pecinka, P. *Electroanalysis* **2006**, *18*, 141–51.
(41) Mittelmann, A. S.; Ron, E. Z.; Rishpon, J. *Anal. Chem.* **2002**, 74, 903–7.
(42) (a) Gyss, C.; Bourdillon, C. *Anal. Chem.* **1987**, *59*, 2350–5. (b) Bourdillon, C.; Demaille, C.; Moiroux, J.; Savéant, J-M. *J. Am. Chem. Soc.* **1999**, *121*, 2401–8.
(43) Limoges, B.; Mavré, F.; Marchal, D.; Savéant, J.-M. *J. Am. Chem. Soc.* **2008**, *130*, 7276–7285.
(44) Neutravidin, a deglycosylated form of avidin, was preferred to avidin itself because it minimizes nonspecific absorption effects.
(45) With the aim to fill the spaces remaining vacant on the electrode after adsorption of b-IgG and thus to minimize nonspecific adsorption during the recognition step, the electrode is exposed to bovine serum albumin (BSA) (see Scheme 2).

Scheme 2

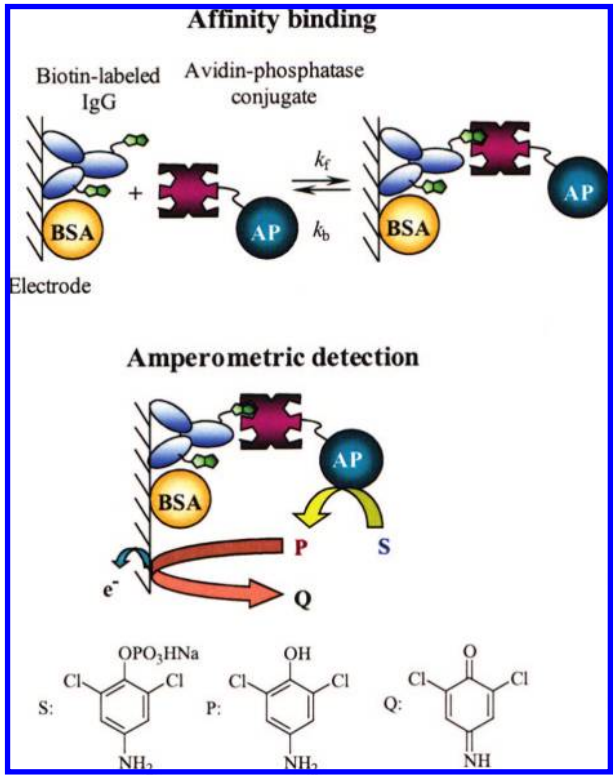

electrochemical detection of the activity of the AP label specifically attached on the electrode surface.

The reason for selecting alkaline phosphatase was its ability to rapidly convert a substrate (S) into an electrochemically detectable product (P). This is also why AP has been widely used as an enzyme label in numerous amperometric enzyme immunosensors[5,14–27] or DNA-sensors[28–41] and is at the origin of some of the most sensitive enzyme-amplified biosensing applications. AP catalyzes the hydrolysis of aromatic monoester phosphates to give phenolic derivatives and an inorganic phosphate. A broad range of aromatic monoester phosphate substrate/phenolic product couples has thus been proposed for the electrochemical detection of AP and consequently applied to electrochemical enzyme affinity assays.

Among these substrate/product couples, the *p*-aminophenyl phosphate (PAPP)/*p*-aminophenol (PAP) couple has been found to be the most advantageous because of the reversible redox behavior of the PAP product at a bare electrode, taking place at a low potential (formal potentials: 0.1 V vs SCE at pH 9), and also because of its low propensity to foul the electrode surface compared to other phenolic products.[46–49] However, as shown in the present report, the electrochemical behavior of PAP is strongly affected by the presence of macrobiomolecules on the electrode surface, leading to a poorly reversible cyclic voltammetric wave endowed with an apparent heterogeneous electron transfer rate significantly lower than at a bare electrode. We have found that 4-amino-2,6-dichlorophenol (2,6-DCPAP)

(46) Frew, J. E.; Foulds, N. C.; Wilshere, J. M.; Forrow, N. J.; Green, M. J. *J. Electroanal. Chem.* **1989**, *266*, 309–16.
(47) Wilson, M. S.; Rauh, R. D. *Biosens. Bioelectron.* **2004**, *20*, 276–83.
(48) Kreuser, M. P.; O'Sullivan, C. K.; Guilbault, G. G. *Anal. Chim. Acta* **1999**, *393*, 95–102.
(49) Tang, H. T.; Lunte, C. G.; Halsall, H. B.; Heineman, W. R. *Anal. Chim. Acta* **1988**, *214*, 187–95.

Scheme 3

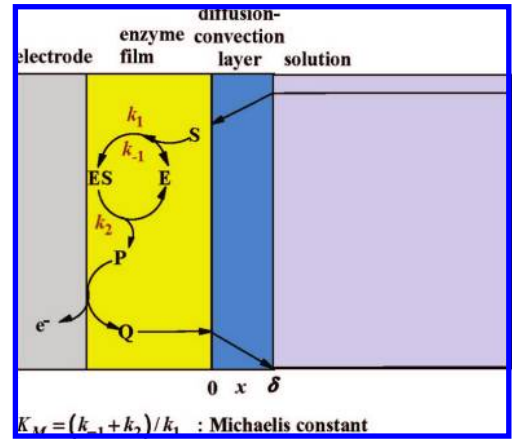

behaves more satisfactorily in this respect. We have thus synthesized the parent AP substrate, 4-amino-2,6-dichlorophenyl phosphate (2,6-DCPAPP or S), and used it to illustrate the theoretical analysis, determine the affinity binding constant, and characterize the electroanalytical performances of the enzyme affinity electrodes toward the quantitative detection of AP-conjugated avidin, as depicted in Scheme 2. The AP label specifically bonded to the electrode was determined by both amperometry and cyclic voltammetry through the electrochemical oxidation of the enzyme generated 2,6-DCPAP product (P) into a 2,6-dichloro-quinonimine (2,6-DCQI or Q) at potentials that do not interfere with the irreversible oxidation of the substrate S. The kinetic parameters of the enzymatic dephosphorylation were determined in homogeneous solution and were used to estimate, from the steady-state amperometric response or the voltammetric peak current, the amount of AP bonded onto the electrode and its maximal coverage. To check the assumption that the kinetic and activity of AP immobilized onto the electrode is the same as in a homogeneous solution, the AP coverage at saturation was also determined by an indirect method. Addressing the important problem of the blank current response in the absence of AP led us to examine the purity and stability of both the substrate 2,6-DCPAPP and the product 2,6-DCPAP.

On the basis of the parameters that emerge from the theoretical analysis the analytical performances are then discussed so as to relate their progressive improvement to the degree of sophistication of the technique (from steady-state chronoamperometry to cyclic voltammetry) and of the cell (from conventional cells to low volume-to-surface ratio cells) and compared with the performances of nonelectrochemical approaches. These parameters also help to optomize the choice of the enzyme by means of the kinetic characteristics they contain.

Results and Discussion

1. Theoretical Relationships. 1.1. Chronoamperometric Response under Steady State Natural Convection/Diffusion Conditions. We consider that, in the absence of stirring, a steady-state current is rapidly established after applying the potential on account of the natural convection that takes place in solution. The diffusion-reaction problem is thus as sketched in Scheme 3. The electrode potential is poised at a value sufficiently positive for the concentration of the enzyme-generated product P to be equal to zero at the electrode surface. The enzyme

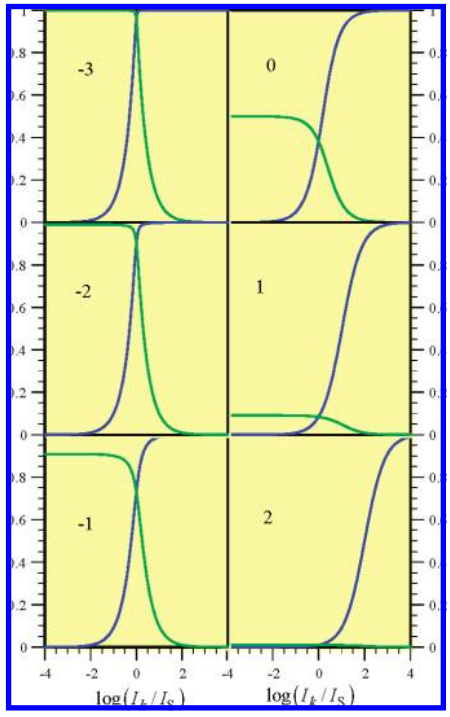

Figure 1. Variations of the current density, under the form of I/I_k (green) or I/I_S, (blue), according to eq 3 and 3′, with the two parameters I_k/I_S, and K_M/C_S^0 (the number in each diagram is the value of $\log(K_M/C_S^0)$)

kinetics is assumed to comply with the classical Michaelis–Menten format, where E designates the free enzyme and ES the intermediate enzyme–substrate complex. The notations for the rate constants are indicated in the scheme.

In a first step, we look for the relationship that links the current density, I, to the surface concentration of the recognized enzyme-labeled analyte, Γ_E^0. We consider that the concentration of substrate and/or the volume of solution are large enough for its consumption in the bulk to be negligible. The current may then be expressed by

$$\begin{aligned}\frac{I}{2F} &= -D_Q\left(\frac{d[Q]}{dx}\right)_{x=0} \\ &= D_S\left(\frac{d[S]}{dx}\right)_{x=0} \\ &= k_1[S]_{x=0}\Gamma_E - k_{-1}\Gamma_{ES} \\ &= k_2\Gamma_{ES}\end{aligned}$$

where D is the diffusion coefficient of the subscript species, [ ] represents the corresponding concentration, and Γ is the surface concentration of the two forms of the enzyme. The subscript $x = 0$ indicates that the concentrations and fluxes are taken at the electrode or at the enzyme layer. The two corresponding average planes may be confounded since the thickness of the enzyme film is small as compared to the diffusion layer (the thicknesses in Scheme 3 are arbitrary). The factor 2 in the first member of the above equation is a stoichiometric factor expressing the fact that the electrochemical oxidation of the product consumes two electrons per molecule as in the illustrating example below and in a number of other cases.

As soon as it is formed at the electrode surface by the enzymatic reaction, the product P is oxidized into Q owing to the poising of the electrode potential at a value positive enough for its concentration to be zero there, thus preventing any diffusion toward the solution. As indicated in the above equation, the enzyme kinetics is assumed to obey the steady state approximation, and since $\Gamma_{ES} + \Gamma_E = \Gamma_E^0$

$$\Gamma_{ES} = \Gamma_E^0\frac{[S]_{x=0}}{K_M + [S]_{x=0}}$$

Therefore,

$$\frac{I}{2F} = k_2\Gamma_E^0\frac{[S]_{x=0}}{K_M + [S]_{x=0}}$$

The substrate concentration at the electrode surface may be expressed as a function of the current as

$$\frac{[S]_{x=0}}{C_S^0} = 1 - \frac{I}{\frac{2FD_SC_S^0}{\delta}}$$

where C_S^0 is the substrate bulk concentration and δ is the thickness of the natural convection/diffusion layer. The term

$$I_S = \frac{2FD_SC_S^0}{\delta} \qquad (1)$$

is the plateau current density of the substrate that would be observed if it were directly oxidized at the electrode. Thus

$$\frac{I}{I_S} = \frac{I_k}{I_S}\frac{1 - \frac{I}{I_S}}{\frac{K_M}{C_S^0} + 1 - \frac{I}{I_S}}$$

where besides the substrate diffusion current density, a current density, I_k, characterizing the enzymatic kinetics

$$I_k = 2Fk_2\Gamma_E^0 \qquad (2)$$

has been introduced

$$\left(\frac{I}{I_S}\right)^2 - \left(\frac{K_M}{C_S^0} + \frac{I_k}{I_S}\right)\frac{I}{I_S} + \frac{I_k}{I_S} = 0$$

or, alternatively, if the current density is normalized toward the enzyme kinetic current density, I_k, rather than toward the substrate diffusion current density:

$$\left(\frac{I}{I_k}\right)^2\frac{I_k}{I_S} - \left(1 + \frac{K_M}{C_S^0} + \frac{I_k}{I_S}\right)\frac{I}{I_k} + 1 = 0$$

Two competition parameters thus emerge from the above equations, K_M/C_S^0, related to the Michaelis–Menten kinetic competition and $I_k/I_S = k_2\Gamma_E^0\delta/D_SC_S^0$, which measures the competition between the substrate diffusion and enzyme kinetics.

Examples of variations of the current density, under the form of I/I_k, or I/I_S, with the two parameters are shown in Figure 1. Increasing the bulk substrate concentration decreases each parameter leading to a limiting situation where the current is solely governed by a saturated Michaelis–Menten kinetics with no interference of substrate diffusion:

$$I = I_k = 2Fk_2\Gamma_E^0$$

This is the best situation for maximizing the current response for a given enzyme. If this limiting situation is not reached, one may use the more complete relationships, which may be recast as

$$\frac{I}{I_S} = \frac{1 + \frac{K_M}{C_S^0} + \frac{I_k}{I_S} - \sqrt{\left(1 + \frac{K_M}{C_S^0} + \frac{I_k}{I_S}\right)^2 - 4\frac{I_k}{I_S}}}{2} \quad (3)$$

or

$$\frac{I}{I_k} = \frac{1 + \frac{I_S}{I_k}\frac{K_M}{C_S^0} + \frac{I_S}{I_k} - \sqrt{\left(1 + \frac{I_S}{I_k}\frac{K_M}{C_S^0} + \frac{I_S}{I_k}\right)^2 - 4\frac{I_S}{I_k}}}{2} \quad (3')$$

It is noteworthy that even when K_M/C_S^0 is small as in the left-hand diagrams in Figure 1, the rate-control passes from enzymatic kinetics to substrate diffusion upon increasing I_k/I_S. The transition between one kinetic control and the other is the sharper the smaller K_M/C_S^0 is.

Another limiting situation of interest is when I_k/I_S is small and K_M/C_S^0 is not particularly small (a situation that can be reached for low surface concentration of the enzyme-labeled analyte, Γ_E^0). The current density is then given by

$$I = I_k \frac{C_S^0}{K_M + C_S^0} = 2Fk_2\Gamma_E^0 \frac{C_S^0}{K_M + C_S^0} \quad (4)$$

Once the relationship between the current density and the surface concentration of the recognized labeled target analyte has been established, the surface concentration can be related to its bulk concentration during the affinity-binding step. The recognition isotherm (for example, but not necessarily,[43] a Langmuir isotherm) may thus be obtained, leading to the determination of the binding equilibrium constant. Relating finally the current density to the solution concentration of the labeled target analyte will allow the estimation of the analytical performances of the method.

1.2. Cyclic Voltammetry at High Volume-to-Surface Ratios. An alternative approach consists in letting the enzyme produce the product P under steady-state natural convection/diffusion conditions and then to sample the production of P by means of cyclic voltammetry as sketched in Scheme 4, under conditions where the scan rate is large enough for the thickness cyclic voltammetry diffusion layer, $(DRT/Fv)^{1/2}$ (D is the value of the diffusion coefficient of P, which is assume to be approximately equal to the diffusion coefficient of Q), to be small compared to that of the steady state natural convection/diffusion layer, δ. A scan rate not larger than 0.1 V/s is usually sufficient for this condition to be fulfilled. For example, if δ is as small as 0.01 cm, it leads for $v = 0.1$ V/s and $D = 4 \times 10^{-6}$ cm^2 s^{-1} to $\delta/(DRT/Fv)^{1/2} = 10$. Under such conditions the peak current is proportional to the steady state concentration of P at the electrode surface, which is related to the various parameters of the system as follows. Unlike the situation in section 1.1, P is not oxidized at the electrode and therefore diffuses in the solution. The steady-state production of P equals the consumption of the substrate S according to[50]

Scheme 4

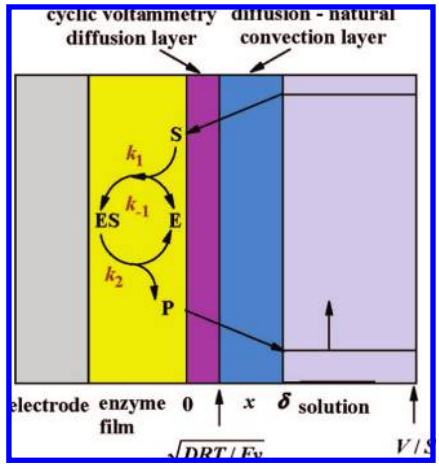

$$\begin{aligned} -D\left(\frac{d[P]}{dx}\right)_{x=0} &= D_S\left(\frac{d[S]}{dx}\right)_{x=0} \\ &= k_1[S]_{x=0}\Gamma_E - k_{-1}\Gamma_{ES} = k_2\Gamma_{ES} \end{aligned} \quad (5)$$

As before,

$$\Gamma_{ES} = \Gamma_E^0 \frac{[S]_{x=0}}{K_M + [S]_{x=0}}$$

and

$$D_S\left(\frac{d[S]}{dx}\right)_{x=0} = k_2\Gamma_E^0 \frac{[S]_{x=0}}{K_M + [S]_{x=0}} = D_S\frac{C_S^0 - [S]_{x=0}}{\delta}$$

Thus

$$\frac{I_k}{I_S}\frac{\frac{[S]_{x=0}}{C_S^0}}{\frac{K_M}{C_S^0} + \frac{[S]_{x=0}}{C_S^0}} = 1 - \frac{[S]_{x=0}}{C_S^0}$$

I_S and I_k being defined by eqs 1 and 2, respectively. From eq 5,

$$D_S(C_S^0 - [S]_{x=0}) = D([P]_{x=0} - [P]_{x=\delta})$$

finally leading to

$$[P]_{x=0} = [P]_{x=\delta} + \frac{D_S C_S^0}{D}\frac{1 + \frac{K_M}{C_S^0} + \frac{I_k}{I_S} - \sqrt{\left(1 + \frac{K_M}{C_S^0} + \frac{I_k}{I_S}\right)^2 - 4\frac{I_k}{I_S}}}{2} \quad (6)$$

As before, an interesting limiting situation, reached upon increasing the bulk substrate concentration, is when the process is solely governed by a Michaelis–Menten saturated kinetics with no interference of substrate diffusion. Then

$$[P]_{x=0} = [P]_{x=\delta} + \frac{k_2\Gamma_E^0\delta}{D} \quad (7)$$

With conventional cells, the volume-to-electrode surface area ratio is large, that is, (see Scheme 4) $(DRT/Fv)^{1/2} \ll \delta \ll V/S$. If the last condition is such that $(V/S)(\delta/D)$ is large as compared to the time during which the experiment is carried out, the building up of P in the solution is negligible (see section 1.3):

$$[P]_{x=\delta} = 0$$

and

$$[P]_{x=0} = \frac{D_S C_S^0}{D}\frac{1 + \frac{K_M}{C_S^0} + \frac{I_k}{I_S} - \sqrt{\left(1 + \frac{K_M}{C_S^0} + \frac{I_k}{I_S}\right)^2 - 4\frac{I_k}{I_S}}}{2}$$

(50) Savéant, J.-M. *Elements of Molecular and Biomolecular Electrochemistry*; Wiley Intersciences: Hoboken, NJ, 2006.

which becomes: $[P]_{x=0} = k_2\Gamma_E^0\delta/D$ under saturated Michaelis–Menten kinetic control.

Under the conditions already defined, the cyclic voltammetric peak current is simply proportional to $[P]_{x=0}$ in all cases:

$$I_p = A \times F\sqrt{D}\sqrt{\frac{Fv}{RT}}[P]_{x=0}$$

The proportionality factor A depends on the electron stoichiometry and of the degree of reversibility of the P wave. These waves, corresponding to a two-electron−two-proton stoichiometry in most cases, are usually not very reversible (for a two-electron irreversible process with a transfer coefficient of 0.5, $A \approx 0.07$). This sluggish reversibility is especially observed when proteins are adsorbed on the electrode. The best way for determining A is to carry out a cyclic voltammetric experiment with a known concentration of P in the solution, with the same coating of the electrode surface, but in the absence of the substrate, that is, in the absence of catalytic reaction.

In summary, the peak current is given by:

$$I_p = A \times F\sqrt{D}\sqrt{\frac{Fv}{RT}}\frac{D_S C_S^0}{D} \times \frac{1 + \frac{K_M}{C_S^0} + \frac{I_k}{I_S} - \sqrt{\left(1 + \frac{K_M}{C_S^0} + \frac{I_k}{I_S}\right)^2 - 4\frac{I_k}{I_S}}}{2} \quad (8)$$

in the general case and by eq 9 under saturated Michaelis–Menten kinetic control:

$$I_p = A \times F\sqrt{D}\sqrt{\frac{Fv}{RT}}\frac{k_2\Gamma_E^0\delta}{D} \quad (9)$$

1.3. Cyclic Voltammetry at Low Volume-to-Surface Ratios. If the volume (V) to surface (S) ratio is large, as in the preceding case when conventional cells are used, there is no point waiting for an increase of the current with time. This is not the case when the V to S ratio is small. Then P is expected to accumulate with time leading to an increased sensitivity. Three cases should be distinguished according to the relative magnitude of the three characteristic lengths $(DRT/Fv)^{1/2}$, δ, and V/S:

Case a. $(DRT/Fv)^{1/2} \ll \delta \ll V/S$, as in the preceding case, but the characteristic time $(V/S)(\delta/D)$ (see later) is of the same order as the experiment duration. The equations governing the production and mass transport of P are the same as in the preceding case, except that its bulk concentration builds up appreciably with time according to

$$\frac{d[P]_{x=\delta}}{dt} = -\frac{SD}{V}\left(\frac{d[P]}{dx}\right)_{x=\delta\_}$$

(with reference to Scheme 4, $\delta\_$ means approaching δ from the left).

$$\frac{d[P]_{x=\delta}}{dt} = \frac{SD}{V}\frac{[P]_{x=0} - [P]_{x=\delta}}{\delta}$$

Equations 6 and 7 are the initial conditions of P building up, while $[P]_{x=0} - [P]_{x=\delta}$ remains constant over time. Thus

$$[P]_{x=0} = ([P]_{x=0} - [P]_{x=\delta})\left(1 + \frac{SD}{V\delta}t\right)$$

where $[P]_{x=0} - [P]_{x=\delta}$ is given by eqs 6 or 7. In the latter case

$$[P]_{x=0} = \frac{k_2\Gamma_E^0\delta}{D} + \frac{S}{V}k_2\Gamma_E^0 t$$

Under the conditions already defined, i.e., $(DRT/Fv)^{1/2} \ll \delta$, the cyclic voltammetric peak current is simply proportional to $[P]_{x=0}$ in all cases:

$$I_p = A \times F\sqrt{D}\sqrt{\frac{Fv}{RT}}[P]_{x=0}$$

In summary, introducing the characteristic time $(V/S)(\delta/D)$, the peak current is given by eq 10 in the general case, and by eq 11 under saturated Michaelis–Menten kinetic control.

$$I_p = A \times F\sqrt{D}\sqrt{\frac{Fv}{RT}}\frac{D_S C_S^0}{D}\left(1 + \frac{t}{V\delta/SD}\right) \times \frac{1 + \frac{K_M}{C_S^0} + \frac{I_k}{I_S} - \sqrt{\left(1 + \frac{K_M}{C_S^0} + \frac{I_k}{I_S}\right)^2 - 4\frac{I_k}{I_S}}}{2} \quad (10)$$

$$I_p = A \times F\sqrt{D}\sqrt{\frac{Fv}{RT}}\left(\frac{k_2\Gamma_E^0\delta}{D} + \frac{S}{V}k_2\Gamma_E^0 t\right) \quad (11)$$

In all cases, the peak current increases linearly with time. Equation 11 depicts the amplification due to accumulation of the enzyme–product with time and introduces a time constant, $V\delta/SD$, which depends on the geometry of the cell defined by V/S, of the product diffusion coefficient and the thickness of the steady-state convection/diffusion layer.

Case b. $(DRT/Fv)^{1/2} \ll V/S \ll \delta$. Natural convection no longer plays a role in P mass transport. The building up of P concentration is confined within the thickness of the cell. The peak current is thus given by eq 12 under saturated Michaelis–Menten kinetic control.

$$I_p = A \times F\sqrt{D}\sqrt{\frac{Fv}{RT}}\left(\frac{k_2\Gamma_E^0 V}{DS} + \frac{S}{V}k_2\Gamma_E^0 t\right) \quad (12)$$

In this case too, the peak current increases linearly with time. S is the electrode surface area and V is the effective volume within which the diffusion of P actually takes place and may be different from the total volume of the solution in the cell (see section 2.4 for an example). It has been implicitly assumed in the above derivation that an even concentration of P is established across the whole thickness of the cell at time zero. In practice this is obviously not the case, leading to a substantial uncertainty on the location of the time origin, and therefore on the value of the intercept, in the peak current–time plots corresponding to eq 12. Analyses based only on the values of the slope in eq 12 are therefore safer.

Case c. $V/S \ll (DRT/Fv)^{1/2} \ll \delta$. The cell thickness, V/S, is so small that all the P present in the cell is entirely detected by cyclic voltammetry, which then gives rise to a surface wave, which height is proportional to the scan rate rather than to its square root, according to eq 13 under saturated Michaelis–Menten kinetic control.

$$I_p = A' \times \frac{F^2 v}{RT}\left(\frac{k_2\Gamma_E^0 V}{DS} + \frac{S}{V}k_2\Gamma_E^0 t\right) \quad (13)$$

In this case again, the peak current increases linearly with time. The ratio between I_p and $I_{p,0}$ (value of I_p at time $t = 0$) is therefore given by an equation which is formally the same as

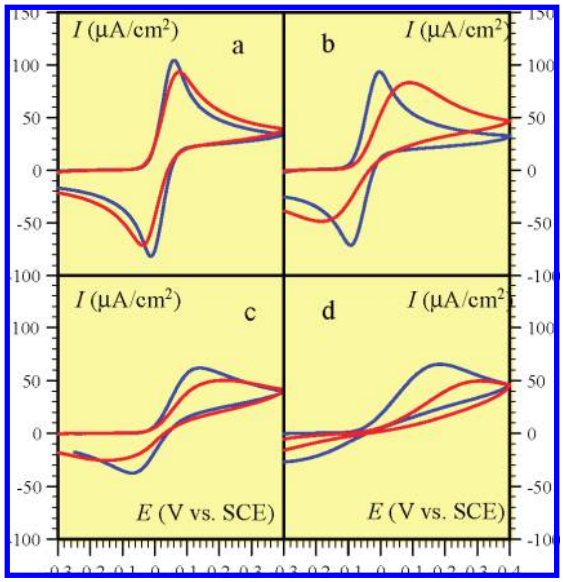

Figure 2. Cyclic voltammetry of 0.1 mM 2,6-dichloro-4-aminophenol and 4-aminophenol in Tris buffer (0.1 M, pH = 9.0) at a bare (blue) or BSA-coated (red) electrode: (a, b) glassy carbon electrode; (c, d) screen-printed electrode. Scan rate = 0.1 V/s.

eq 12. The same remarks as in the preceding case concerning the lack of precision on the value of the intercept and the better reliability of the slope values apply.

One way of achieving these conditions is to decrease more and more the cell thickness. A similar situation is expected when the product P is converted into an electroactive precipitate on the electrode surface as for example by oxidation of P with Ag^+ leading to an Ag precipitate, which can be detected and quantitated electrochemically.[51] However, precipitation has to be quantitative, fast, and harmless for the enzyme functioning over the whole range of target analyte concentrations, a condition that seems difficult to achieve with this technique and other procedures based on precipitation[37,52] as will be discussed on experimental grounds in section 2.4.

1.4. Current, Enzyme Label Surface Concentration, and Target Analyte Bulk Concentration. In all cases, plotting the values of Γ_E^0 versus the bulk concentration of the labeled target analyte at binding equilibrium provides the recognition isotherm (for example, but not necessarily, a Langmuir isotherm) and thus the value of the binding equilibrium constant. Relating finally the peak current to the solution concentration of the labeled target analyte will allow the estimation of the analytical performances of the method.

2. Illustrating Example: Alkaline Phosphatase Amplified Avidin–Biotin Recognition Electrode. 2.1. Selection of the Substrate/Product Couple. Electrochemical and Enzymatic Characterization. Stability and Purity of the Reagents. The electrochemical properties of 2,6-DCPAP were characterized in cyclic voltammetry both at bare carbon electrodes and at carbon electrodes coated with an adsorbed layer of bovine serum albumin (BSA). The resulting voltammograms were also compared with the curves obtained for PAP under the same conditions (Figure 2). Two kinds of carbon-based electrodes were evaluated, glassy carbon and screen-printed carbon electrodes. The latter are particularly valuable in the development of electrochemical enzyme immuno- or DNA-assays, their main advantages being ease of mass production, low-cost, low background current, good reproducibility, and disposable handling. The screen-printing technology also offers a high flexibility in the design and fabrication of multiplexed arrays of electrochemical microcells.

At a bare glassy carbon electrode, the cyclic voltammetry of 2,6-DCPAP (scan rate: 0.1 V s^{-1}) shows a well-defined diffusion-controlled reversible wave, with a formal potential $E^{\circ\prime}$ (average of the anodic and cathodic peak potentials) of +0.024 V vs SCE, and a peak potential difference of $\Delta E_p = 68$ mV, pointing to a relatively rapid overall two-electron transfer, which involves the $2e^- + 2H^+$ oxidation of 2,6-DCPAP into the corresponding quinonimine, 2,6-DCQI:

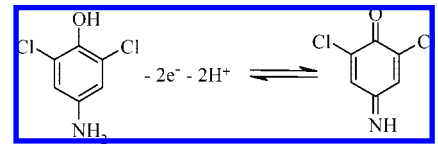

Under the same conditions, the cyclic voltammetry of PAP also gives rise to a well-defined two-electron reversible wave, but with a formal potential slightly more negative than 2,6-DCPAP ($E^{\circ\prime} = -0.048$ V vs SCE) as expected from the electron-withdrawing effect of the two chlorine and an apparent heterogeneous electron transfer rate somewhat slower ($\Delta E_p =$ 88 mV). Coating the electrode with BSA does not change significantly the formal potentials but significantly slow down electron transfer ($\Delta E_p = 115$ mV and 276 mV for 2,6-DCPAP and PAP, respectively) in line with a partial blocking of the electrode by the adsorbed protein molecules. The results were qualitatively similar at screen-printed carbon electrodes, except that electron transfer is further slowed down, which is not surprising in view of the heterogeneous composition of the screen-printed carbon electrode surface, made of a random distribution of closely spaced insulating and conductive microscopic zones. The consequence of this partial blocking of the electrode surface is an increase of the peak-to-peak separation in cyclic voltammetry, reflecting an apparent slowing down of electron transfer kinetics.[53,54] The better electrochemical characteristics of 2,6-DCPAP as compared to PAP on all types of electrodes, led us to select 4-amino-2,6-dichlorophenylphosphate as substrate. This compound was synthesized according to a two-step procedure. The phenolic group was first phosphorylated with dibenzylphosphite in tetrachloromethane,[55,56] and the resulting dibenzylated phosphate ester was next catalytically hydrogenated in the presence of palladium on calcium carbonate (see Experimental Section).

The new substrate was then characterized electrochemically and enzymatically. Cyclic voltammograms of 2,6-DCPAPP (Figure 3a) show during the forward scan an irreversible oxidation peak, and upon scan reversal, the reversible reduction peak followed by the appearance of a reversible system

(51) Hwang, S.; Kim, E.; Kwak, J. *Anal. Chem.* **2005**, *77*, 579–84.
(52) Patolsky, F.; Katz, E.; Bardea, A.; Willner, I. *Langmuir* **1999**, *15*, 3703–6.
(53) Amatore, C.; Savéant, J-M.; Tessier, D. *J. Electroanal. Chem.* **1983**, *147*, 39–51.
(54) Osborne, M. D.; Seddon, B. J.; Dryfe, R. A. W.; Lagger, G.; Loyall, U.; Schäfer, H.; Girault, H. H. J. *Electroanal. Chem.* **1996**, *417*, 5–15.
(55) Silverberg, L. J.; Dillon, J. L.; Vemishetti, P. *Tetrahedron Lett.* **1996**, *37/6*, 771–4.
(56) Authier, L.; Schöllhorn, B.; Moiroux, J.; Limoges, B. *J. Electroanal. Chem.* **2000**, *488*, 48–58.

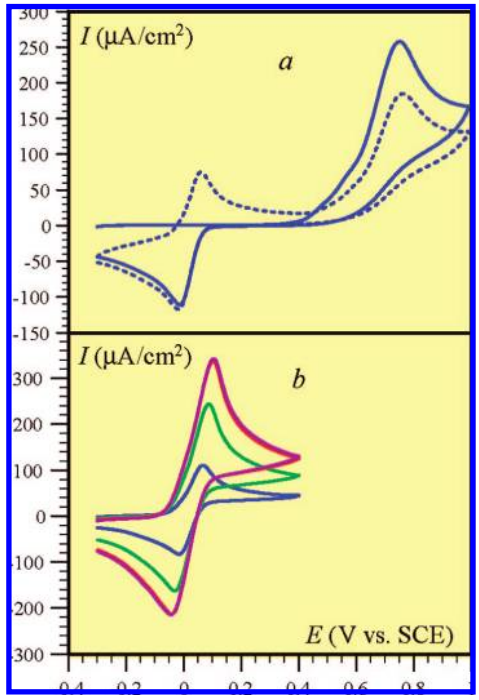

Figure 3. (a) Cyclic voltammograms: [(—) first scan, (...) second scan] recorded at a glassy carbon electrode immersed in a 0.1 M Tris buffer (pH 9.0) containing 1 mM 2,6-DCPAPP and 1 mM $MgCl_2$. (b) After addition of 20 nM AP and after a few seconds (blue), 1 min (green), 3 min (red), and 5 min (magenta). Scan rate = 0.1 V/s; starting potential = −0.3 V vs SCE.

Scheme 5

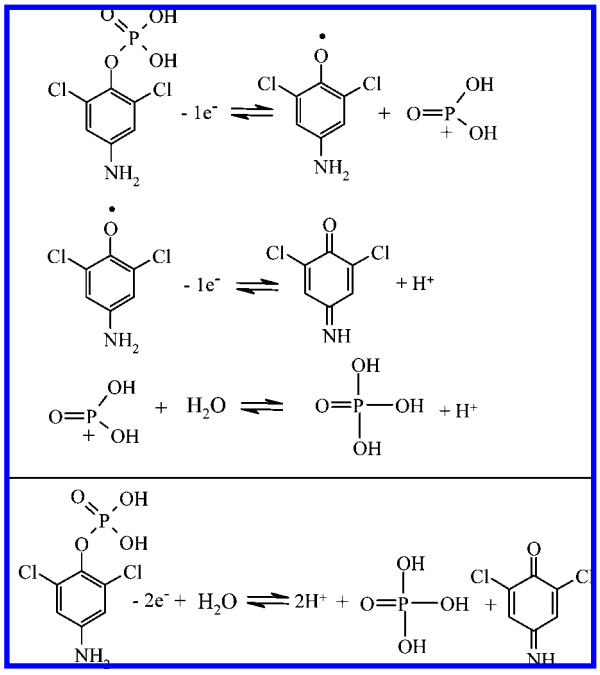

corresponding to the reduction of 2,6-DCQI. These observations point to the following reaction scheme (Scheme 5).[57]

It is worth noting the absence of oxidation wave at ~0.06 V during the first anodic scan, pointing to a very low level of residual traces of 2,6-DCPAP in the synthesized substrate. The difference between the oxidation peak potentials of 2,6-DCPAP and 2,6-DCPAPP is quite large (ΔE = 0.68 V), larger than between PAP and PAPP (ΔE = 0.46 V)[49,58] or between 4-aminonaphtol and 4-aminonaphtylphosphate (ΔE = 0.46 V).[59] This is an important advantage for increasing the selective electrochemical oxidation of 2,6-DCPAP without interference from the electrochemical oxidation of the 2,6-DCPAPP substrate. The problem of an insufficient discrimination between the substrate and product detection has already been identified with the PAP/PAPP couple as a source of significant background current, hindering the improvement of the detection limit of the method.[35]

The ability of alkaline phosphatase to hydrolyze the new substrate is illustrated in Figure 3b. Incubation of the 1 mM substrate solution in the presence of an excess of AP (20 nM), leads to a nearly complete conversion of 2,6-DCPAPP to 2,6-DCPAP product in less than 5 min. Hydrolysis follows a simple Michaelis–Menten mechanism. The two pertinent kinetic parameters k_2 and K_M in solution could thus be determined, spectrophotometrically (k_2 = 1837 s^{-1}, K_M = 48 μM) and electrochemically (k_2 = 1100 s^{-1}, K_M = 67 μM) by measuring the substrate dependence of the rate of reaction at pH 9.0 in 0.1 M Tris containing 1 mM $MgCl_2$, henceforth designated as TB (see Experimental Section), which correspond to the optimal conditions for hydrolysis of PAPP by AP.[60] The K_M is of the same order as for *p*-nitrophenylphosphate (K_M = 82 μM),[60] PAPP (K_M = 56 μM)[60] or phenyl phosphate (K_M = 36 μM).[61] The turnover number is also of the same order as that found for other aromatic monoester phosphates such as *p*-nitrophenylphosphate (k_2 = 1800 s^{-1})[62] or phenyl phosphate (k_2 = 800 s^{-1}).[61]

The N-AP kinetics was also determined electrochemically at pH = 6.5 (MES buffer containing 0.1 wt% BSA and 1 mM $MgCl_2$), leading to k_2 = 45 s^{-1} and K_M = 20 μM.

It has been previously observed that PAP is not very stable in aerated alkaline solutions.[49,60] This instability was ascribed to a slow decomposition of PAP by air-oxidation, as in several other hydroquinone and aminophenol derivatives.[59] Despite a notably higher redox potential and thus a lower susceptibility to air-oxidation, a similar instability was observed with 2,6-DCPAP. It leads, in aerated TB, at pH 9.0, to a continuous decrease of the cyclic voltammetric response with time (Figure 4), which is also related to the presence of dioxygen. The decrease is not caused by electrode passivation since transferring the electrode into a fresh solution of 2,6-DCPAP allows recovering the starting voltammetric response. The rate of decomposition at neutral pH is considerably slower and almost independent of the presence of dioxygen. The moderate instability of 2,6-DCPAP at alkaline pH is however not critical in the chronoamperometric technique defined in section 1.2, since 2,6-DCPAP is generated in the proximity of the electrode surface and electrochemically oxidized as soon as formed.

(57) It may seem at first sight that more electrons are exchanged during the forward anodic scan than during the reverse cathodic scan. This is in fact due to the diffusion toward the solution of the anodic scan product, 2,6-DCQI, during the time elapsed between the anodic and cathodic peaks, as confirmed by simulation of the voltammogram.

(58) Xu, Y.; Halsall, H. B.; Heineman, W. R. *J. Pharm. Biomed. Anal.* **1989**, *7*, 1301–11.
(59) Másson, M.; Rúnarsson, O.; Jóhannson, F.; Aizawa, M. *Talanta* **2004**, *64*, 174–80.
(60) Thompson, R. Q.; Barone, G. C., III; Halsall, H. B.; Heineman, W. R. *Anal. Biochem.* **1991**, *192*, 90–5.
(61) Bauer, C. G.; Eremenko, A. V.; Ehrentreich-Förster, E.; Bier, F. F.; Makower, A.; Halsall, H. B.; Heineman, W. R.; Scheller, F. W. *Anal. Chem.* **1996**, *68*, 2453–8.
(62) Ciana, L. D.; Bernacca, G.; Bordin, F.; Fenu, S.; Garetto, F. *J. Electroanal. Chem.* **1995**, *382*, 129–135.

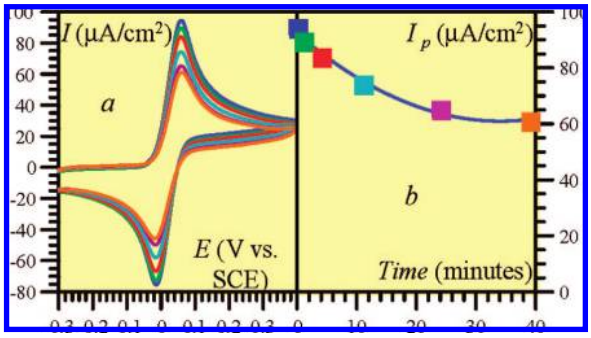

Figure 4. (a) Cyclic voltammograms of 2,6-DCPAP (0.1 mM in aerated 0.1 M Tris buffer, pH 9.0) recorded at different time intervals after immersion of the glassy carbon electrode in the freshly prepared solution. Scan rate = 0.1 V/s. (b) Decay of the voltammetric anodic peak current (from a) as a function of time. Color codes are the same in a and b.

The amount of residual traces of 2,6-DCPAP contained in the solid substrate powder was estimated in cyclic voltammetry from the anodic peak current recorded at ~0.1 V at a glassy carbon electrode immersed in a series of fresh solutions of 1 or 10 mM 2,6-DCPAPP in TB. Less than 0.05% of 2,6-DCPAP was estimated to be present in the synthesized 2,6-DCPAPP. The stability of the substrate 2,6-DCPAPP to spontaneous hydrolysis in alkaline buffer was also monitored by the evolution with time of the residual voltammetric peak current corresponding to 2,6-DCPAP in a solution of 1 mM 2,6-DCPAPP in TB. The fact that it is practically constant after several hours in TB suggest either that the spontaneous hydrolysis of 2,6-DCPAPP is very slow or, alternatively, that the slow formation of 2,6-DCPAP is compensated by its decomposition.

2.2. Chronoamperometric Responses under Steady State Natural Convection/Diffusion Conditions. A series of screen-printed carbon electrodes were coated with a saturated monolayer of b-IgG by means of an irreversible adsorption of the protein on the surface of the electrode. Nonspecific adsorption during the N-AP binding step was minimized by a follow-up blocking of the unoccupied sites on the electrode surface with bovine serum albumin (BSA). The b-IgG-modified screen-printed carbon electrodes, thus prepared, were incubated overnight in N-AP solutions of different standard concentrations ($C^0_{\text{N-AP}}$) at room temperature. Relatively long times are indeed required to ensure that the binding of N-AP to the b-IgG-modified electrode has reached equilibrium, even at the lowest N-AP concentrations (it was checked that, for the lowest concentrations, prolonged incubation times lead to the same limiting current responses). The binding recognition was also achieved in a large volume of N-AP solution in such a way that there is no significant N-AP depletion in the analyte solution ($C^0_{\text{N-AP}} \approx$ constant). Once equilibrium binding was reached, the electrodes were washed and immersed in the enzyme–substrate solution (2 mL of TB containing 1 mM 2,6-DCPAPP) for steady-state chronoamperometric measurements. Typical chronoamperometric responses obtained with a series of b-IgG-modified screen-printed carbon electrodes incubated with different standard N-AP concentrations, which cover a range extending from 2 to 2×10^5 picomol/liter are shown in Figure 5. The chronoamperometric measurements were recorded at 0.25 V versus SCE, a potential sufficiently positive to efficiently oxidize 2,6-DCPAP but not too high so as to avoid the direct oxidation of the substrate. The steady-state currents, reached after some tens of seconds, result from natural convection in the solution, which leads to the formation of a steady-state diffusion−convection layer. The thickness of the diffusion−convection layer may be estimated independently from the steady-state chronoamperometric response of a standard solution of 2,6-DCPAP. The steady-state current density being expressed as $I = 2FDC^0_P/\delta$, it follows that $D/\delta \approx D_S/\delta = (2.1 \pm 0.3) \times 10^{-4}$ cm/s.

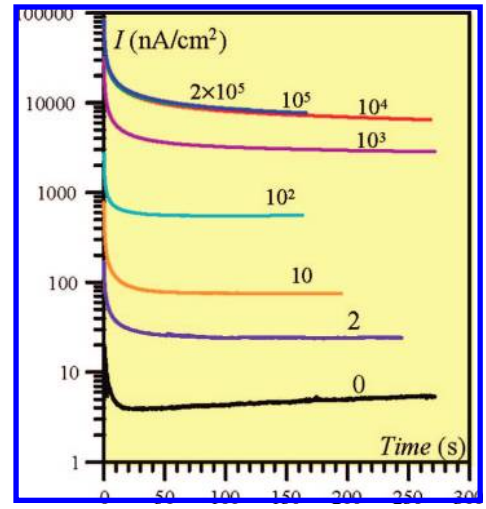

Figure 5. Chronoamperometric current density responses recorded at b-IgG-coated screen-printed electrodes incubated overnight at room temperature in solutions containing different concentrations of N-AP. Applied potential: 0.25 V vs SCE. The solution contains a 0.1 M Tris buffer (pH 9.0), 1 mM $MgCl_2$ and 1 mM of 2,6-DCPAPP. The number on each curve is the N-AP bulk concentration expressed in picomol/liter.

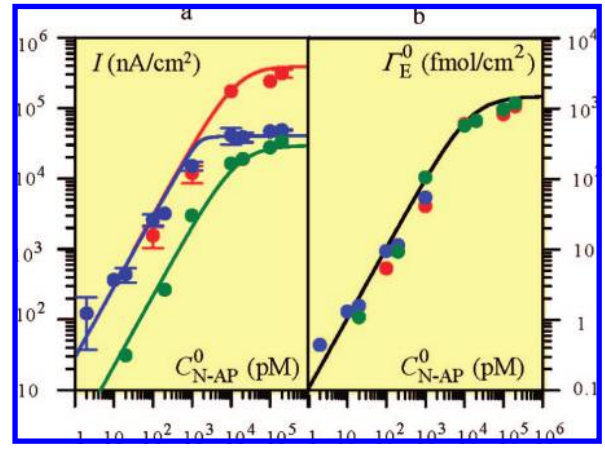

Figure 6. (a) Variations of the steady-state chronoamperometric current density responses, at a b-IgG-coated screen-printed electrode, with the solution concentration of the enzyme-labeled analyte. The currents were recorded at pH = 9 (red and blue dots) and pH = 6.5 (green dots) in solutions containing 10 mM (red dots) and 1 mM (blue and green dots) of the substrate 2,6-DCPAPP. Other conditions are the same as in Figure 5. All data were corrected from the average blank response obtained at $C^0_{\text{N-AP}} = 0$. Error bars represent the standard deviation. (b) Variation of the surface concentration of the recognized enzyme-labeled analyte as a function of its solution concentration during incubation. Solid lines are simulations according to the theoretical relationships of section 1.1 (see text).

The steady state current densities thus obtained were plotted against $C^0_{\text{N-AP}}$ in Figure 6 (blue dots), after correction from the average blank response. The latter was obtained by measuring the current responses at a series of b-IgG-coated electrodes immersed in the enzyme–substrate solution without preincubation in a N-AP solution ($C^0_{\text{N-AP}} = 0$). Repeated experiments showed that the standard deviation on the determination of the

average blank current density is $\Delta I = \pm 20$ nA/cm^2. In addition, it was verified that the nonspecific adsorption of N-AP is rendered negligible by the presence of BSA on the electrode surface by measuring the current response at electrodes coated with BSA only and incubated in a N-AP solution of relatively high concentration (5×10^{-10} M). A nonspecific current response corresponding to 0.1% of the specific current response was obtained, indicating a relatively low nonspecific binding. The resulting curve has roughly the shape of a recognition isotherm, although the transition between the ascending linear portion and the horizontal asymptote is steeper than in a Langmuir isotherm. That it is not a true recognition isotherm results from another series of similar experiments carried out at a larger substrate concentration (red dots), 10 mM instead of 1 mM. The ensuing curve does not change upon further increase of the substrate concentration, showing that the partial control by substrate diffusion, present in the blue-dot experiments, vanished in the red-dot experiments as the parameter $I_k/I_S = k_2\Gamma_E^0\delta/D_S C_S^0$ decreases upon increasing C_S^0.

This conclusion falls in line with the observation that the red and blue dots fall on the same line at lower values of $C_{N\text{-}AP}^0$(pM), hence of Γ_E^0, which also results in a decrease of the parameter I_k/I_S. The whole red-dot data and the low-concentration range blue-dot data may thus be safely treated as representing the avidin–biotin recognition isotherm on the electrode surface. The limiting value of the current density at large values of $C_{N\text{-}AP}^0$ corresponds to the maximal enzyme coverage, $\Gamma_{E,max}^0$. Since the process is entirely governed by the enzyme kinetics, as just ascertained, application of eq 2 leads to $I = I_{k,max} = 2Fk_2\Gamma_{E,max}^0$ and thus to $k_2\Gamma_{E,max}^0 = 2 \times 10^{-9}$ mol cm^{-2} s^{-1}. Assuming that k_2 is the same as in homogeneous solution (i.e., $k_2 = 1500$ s^{-1}, taking the average between the spectrophotometric and electrochemical determinations), $\Gamma_{E,max}^0 = 1500$ fmol cm^{-2}. This value agrees with the coverage that can be estimated from protein sizes for a saturated monolayer on a perfectly flat surface (1700 fmol cm^{-2}). This result was corroborated by additional experiments that allow the determination of $\Gamma_{E,max}^0$ independently from k_2. The method is the same as the "depletion method" formerly used with horseradish peroxidase.[63] It consists in depositing a droplet of N-AP solution on the surface of the b-IgG-modified electrode and determining spectrophotometrically, after an incubation period, the remaining activity of the enzyme contained in the droplet. On account of the large ratio of electrode surface/droplet volume, a sizable amount of N-AP is depleted from the drop. This amount of enzyme normalized toward the surface area corresponds to the amount specifically bound to the electrode surface. Using this method with a saturating concentration of N-AP a value of $\Gamma_{E,max}^0 = 1500 \pm 300$ fmol cm^{-2} was found in agreement with the previous determination.

From the value of the proportionality factor, $2Fk_2$, between I_k and Γ_E^0, and considering that one phosphatase is coupled to one neutravidin, we may then derive the whole recognition isotherm as shown in Figure 6b. Fitting with a Langmuir curve

$$\Gamma_E^0 = \Gamma_{E,max}^0 \frac{K_b C_{N\text{-}AP}^0}{1 + K_b C_{N\text{-}AP}^0} \qquad (14)$$

leads to a binding constant, $K_b = 7 \times 10^7$ M^{-1}. This value is much lower than the constants reported for the binding of native biotin with avidin (1.7×10^{15} M^{-1}) or streptavidin (2.5×10^{13} M^{-1}) in homogeneous solution,[64,65] in line with the observation made with fluorescent-labeled biotins showing that the nature and length of the structure that links the biotin to the fluorescent probe affect significantly the binding with avidin.[66–68] For example, homogeneous binding constants values ranging from 10^8 to 10^{10} M^{-1} have been reported, which is about 5–7 orders of magnitude lower than the native biotin for avidin.[66–68] A similar decrease in the affinity for avidin can be anticipated in the present case for the binding of large biotinylated proteins such as b-IgG. An additional factor might be a lesser access to the immobilized biotin ligand at the electrode surface or a steric hindrance of available sites by bound N-AP.[69]

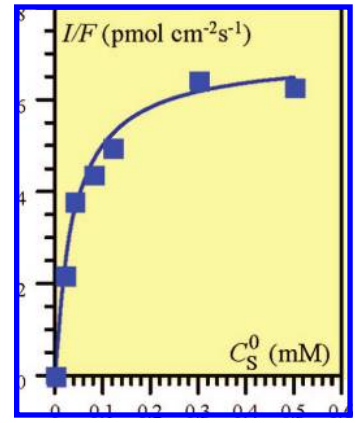

Figure 7. Michaelis–Menten plot of the steady-state chronoamperometric current density responses as a function of 2,6-DCPAPP concentrations recorded at a b-IgG-modified electrode loaded with a low amount of N-AP (i.e., obtained after incubation in a solution of 30 pM N-AP). Other conditions are the same as in Figure 5.

Further evidence that immobilized N-AP has the same reactivity as in homogeneous solution was obtained by measuring the Michaelis–Menten constant of the immobilized enzyme. At low N-AP coverages, as in the experiments reported in Figure 7, eq 4 indeed applies leading to a K_M value of 40 μM. This value is close to that measured for N-AP in homogeneous solution ($K_M = 48$ μM) by means of steady-state spectrophotometry (section 2.1).

Coming back to the blue-dot data in Figure 6a, simulation that takes into account a partial control by substrate diffusion according to eq 3 leads to a satisfactory fitting of the experimental data using already determined parameters, namely $k_2 = 1500$ s^{-1}, $K_M = 50$ μM, $D_S/\delta = 2.1 \times 10^{-4}$ cm/s, $K_b = 7 \times 10^7$ M^{-1}, $\Gamma_{E,max}^0 = 1500$ fmol cm^{-2}

The applicability of the theoretical relationships may be further tested with the data obtained at pH = 6.5 (green dots in Figure 6) where the enzymatic reaction is expected to be slower than at pH = 9. This is indeed the case with the consequence that, even with a substrate concentration of 1 mM, the enzymatic kinetics governs the current over the whole range of N-AP

(63) Limoges, B.; Savéant, J-M.; Yazidi, D. *J. Am. Chem. Soc.* **2003**, *125*, 9192–203.
(64) Green, N. *Biochem. J.* **1963**, *89*, 585–91.
(65) Bayer, E. A.; Wilcheck, M. *Methods Biochem. Anal.* **1980**, *26*, 1–45.
(66) Lo, K. K.-W.; Chan, J. S.-W.; Lui, L.-H.; Chung, C.-K. *Organometallics* **2004**, *23*, 3108.
(67) Marek, M.; Kaiser, K.; Gruber, H. J. *Bioconjugate Chem.* **1997**, *8*, 560–6.
(68) Loosli, A.; Rusbandi, U. E.; Gradinaru, J.; Bernauer, K.; Schlaepfer, C. W.; Meyer, M.; Mazurek, S.; Novic, M.; Ward, T. R. *Inorg. Chem.* **2006**, *45*, 660–8.
(69) Huang, S.-C.; Stump, M. D.; Weiss, R.; Caldwell, K. D. *Anal. Biochem.* **1996**, *237*, 115–22.

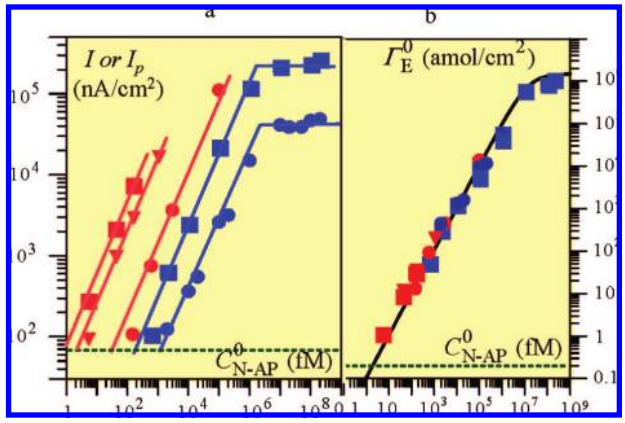

Figure 8. (a) Variations of the (blue dots) steady-state or (blue squares, red dots, squares and triangles) voltammetric peak current density (scan rate: 0.1 V/s) as a function of $C^0_{N\text{-}AP}$. The blue dots and squares were obtained in a conventional cell ($V/S \gg 10$ cm), whereas the red dots, squares, and triangles were obtained in a small volume-to-surface cell ($V/S = 0.25$ cm) after 1 h of enzyme–product accumulation (red dots) or in a thin-layer electrochemical cell ($V/S = 0.006$ cm) after 20 min (red triangles) and 1 h (red squares) of enzyme–product accumulation. The enzyme–substrate solution contains a 0.1 M Tris buffer (pH 9.0), 1 mM $MgCl_2$, and 1 mM of 2,6-DCPAPP. The oblique straight lines are fitted to the linear part of the isotherms (with a slope of 1). The horizontal green dotted line represents 3 times the standard deviation of the average blank response. (b) Variation of the surface concentration of the recognized enzyme-labeled analyte as a function of its solution concentration during incubation. Black solid line is a fitting according to a Langmuir isotherm.

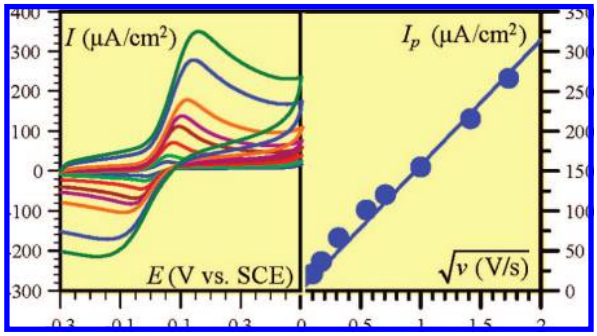

Figure 9. Cyclic voltammetric current density responses at a b-IgG-coated glassy carbon electrode, loaded with a low amount of N-AP (i.e., obtained by incubation in a 100 pM solution of N-AP) and recorded as a function of the scan rate in a standard cell. Other conditions are the same than in Figure 8.

concentrations with no interference of substrate diffusion unlike what was observed at pH = 9. The fitting green curve in Figure 6 was accordingly simply obtained from eq 2, with a value of $k_2 = 110\ s^{-1}$, 10 times lower than at pH = 9, close to the value of the rate constant measured in homogeneous solution at pH 6.5 ($k_2 = 45\ s^{-1}$).

Taking into account this difference in the proportionality factor between current density and surface concentration of the enzyme-labeled analyte, all green and red dots and low concentration blue dots fall on the same $\Gamma^0_E - C^0_{N\text{-}AP}$ curve (Figure 6b), which represents the avidin–biotin recognition isotherm with at saturation a maximal enzyme coverage of $\Gamma^0_{E,max} = 1500$ fmol cm^{-2} and as binding constant of $K_b = 7 \times 10^7\ M^{-1}$.

The fact that the horizontal asymptotes of the blue and green curve in Figure 6 are approximately the same is purely coincidental. It is interesting to note that, in Figure 6a, the approach of the asymptote is almost discontinuous in the blue curve, as expected from the passage from enzyme kinetics control to diffusion control, whereas it is much smoother in the red and green curves as expected from curves that derive from a Langmuir isotherm. This observation brings about a final touch to the excellent agreement between theory and experiment with the testing example that we have chosen.

2.3. Cyclic Voltammetric Responses at High Volume-to-Surface Ratios. Cyclic voltammetric experiments carried out at 0.1 V/s in the same conditions as the blue-dot steady state chronoamperometric experiments reported in Figure 6a are shown in Figure 8 (in which the previous chronoamperometric results are also reported for comparison as well as three series of results obtained with small volume-to-surface cells as described further on).

As before, the average blank current response (mainly due to the faradaic current of residual traces of 2,6-DCPAP present in the substrate solution) was subtracted before plotting the peak current against the concentration of enzyme-labeled analyte. The cyclic voltammetry and chronoamperometry curves are closely parallel, in line with the eqs 3, 3′, and 8. The ratio

$$\frac{I_p}{I} = \frac{A}{2}\sqrt{\frac{Fv}{RT}}\frac{\delta}{\sqrt{D}}$$

is equal to 5.5 for $v = 0.1$ V/s, meaning, from the values already known of all other parameters, that $A \approx 0.6$, very close to the prediction made in section 1.2. The ratio I_P/I could be further improved by raising the scan rate. However, as already mentioned in section 2.1, the quality of the response at screen-printed electrodes rapidly degrades as the scan rate is raised: the coefficient A decreases and the peak shape eventually disappears. Glassy carbon electrodes give more satisfactory results in this connection, as seen in Figure 9, showing that the peak is proportional to the square root of the scan rate.

2.4. Cyclic Voltammetric Responses at Low Volume-to-Surface Ratios. Two cell configurations with a low volume-to-surface ratio were operated.

(a) In a first series of experiments, the production of P from the enzymatic transformation took place in a *droplet* of substrate solution (volume $V = 3 \times 10^{-2}$ cm^3), deposited on top of a b-IgG-coated screen-printed electrode (surface $S = 0.125$ cm^2) that has been previously incubated with a given concentration of enzyme labeled analyte (see the description of the cell in the Experimental Section). The voltammogram of the 2,6-DCPAP produced during the incubation period was then recorded as a function of time (Figure 10a). As shown in Figure 10a′, whatever the amount of enzyme label specifically attached to the working electrode surface, the peak current increases linearly with time. This is precisely what is predicted by eqs 10–12. At prolonged incubation times, it was occasionally observed that the response tends to be higher than predicted (blue data in Figure 10a′). This effect is indicative of concentrating effect due to partial droplet evaporation along the incubation time (during the enzymatic reaction, humidity was not perfectly controlled because of repetitive openings of the chamber between each electrochemical measurement).

From application of eq 12 to the data in Figure 10a′, one obtains $V\delta/SD = 20 \pm 9$ minutes, meaning that the current doubles every 20 min. From this value, with $D/\delta = 2 \times 10^{-4}$ cm/s (determined in the droplet, according to the same procedure as before), one obtains $V/S = 0.25 \pm 0.1$ cm, which is satisfactorily close to the value calculated from the ratio of the geometric area of the electrode and the volume of the deposited droplet ($V/S = 0.24$ cm).[70]

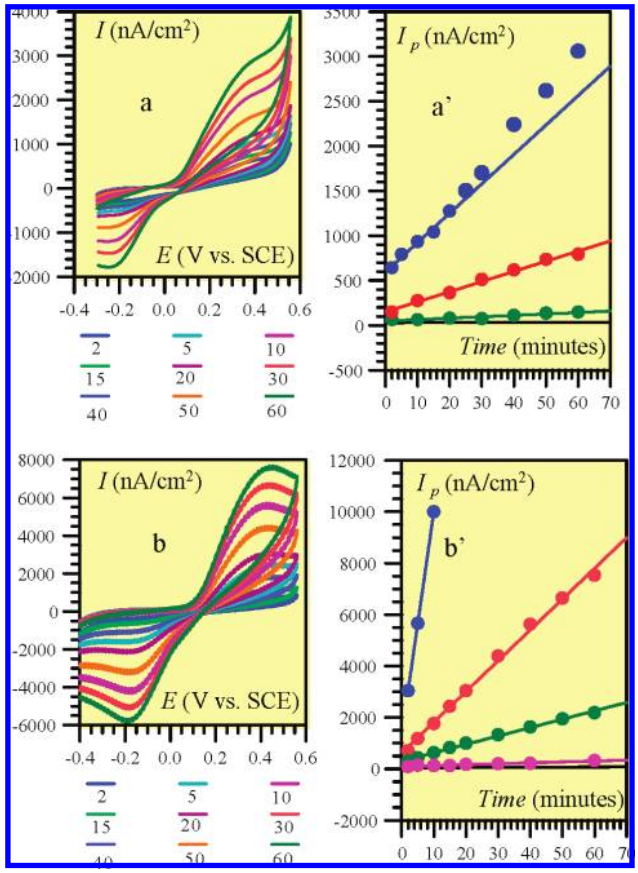

Figure 10. Variations of the cyclic voltammetric current density responses with time after saturation of the electrode with b-IgG, incubation in a solution of N-AP, and exposition to 1 mM 2,6-DCPAPP in TB: (a, a′) droplet cell ($V/S = 0.25$ cm); (b, b′) thin-layer cell ($V/S = 0.006$ cm); (a, b) cyclic voltammograms for $C^0_{N\text{-}AP} = 3000$ and 150 fM, respectively, recorded at different time intervals (indicated in minutes under the diagrams) during the enzyme-generated product accumulation; (a′) peak current density variations for the droplet cell at $C^0_{N\text{-}AP} = 3000$ (blue), 600 (red), 150 (green), 0 (black) fM; (b′) peak current density variations for the thin-layer cell at $C^0_{N\text{-}AP} = 1000$ (blue), 150 (red), 20 (green), 5 (magenta), 0 (black) fM. Scan rate = 0.1 V/s. Straight lines are linear regressions using eqs 11 and 13.

Several other N-AP standard concentrations were similarly investigated and the voltammetric peak currents recorded after one-hour enzyme incubation were reported in Figure 8 as a function of $C^0_{N\text{-}AP}$ (red dots), where they are compared with all the other results. The resulting linear part of the log–log calibration curve (slope = 1) is, as expected, shifted toward lower analyte concentrations, allowing one to reach a lower detection limit compared to previous approaches.

(b) In another series of experiments aiming at a further increase of the analytical performance and at avoiding evaporation of the enzyme–substrate droplet, the enzyme–substrate solution was confined within a *thin-layer* between a planar screen-printed electrochemical cell and a glass coverslip for microscope slide. This was simply done, just prior to the enzyme reaction, by spreading uniformly, with the help of the glass coverslip, a small droplet of substrate solution (4 μL) over all three electrodes (see the description of the cell in the Experimental Section). The adhesive forces between the liquid, the planar electrochemical cell, and the glass coverslip then create an even thickness of liquid of ~60 μm on top of the working electrode, meaning that the ratio of the effective volume to the electrode surface (V_{eff}/S) is of the order of 60 μm. Figure 10b shows a typical series of voltammetric curves recorded during the enzyme–product accumulation within the thin-layer electrochemical cell. The anodic peak currents are reported, as previously, as a function of the enzyme reaction time and for different concentrations of N-AP during the binding recognition step (Figure 10b′).

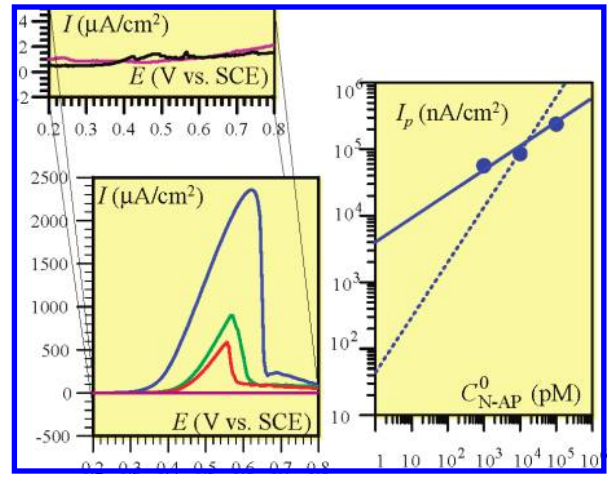

Figure 11. Anodic stripping voltammetry of Ag^0 precipitated on the surface of different N-AP/b-IgG-modified electrodes. During the enzyme reaction the electrode was exposed to a solution containing 1 mM 2,6-DCPAPP and 2 mM $AgNO_3$ for 30 min: (a) anodic stripping voltammograms for $C^0_{N\text{-}AP} = 10^5$ (blue), 10^4 (red), 10^3 (green), 10^2 (magenta, see the zoomed insert), 0 (black) fM; (b) variations of the peak current density with $C^0_{N\text{-}AP}$. Dotted line is the unity slope expected from the Henry's law. Scan rate = 0.1 V/s.

The peak currents obtained after 20 min and 1 h of enzymatic reaction are reported in Figure 8 leading a new calibration curve with enhanced sensitivity. Using this strategy, a concentration as low as 5 fM N-AP was clearly discernible from the blank response.

As discussed in section 1.3, eq 13 cannot be safely used for the estimation of V_{eff}/S in view of the uncertainty on intercept determination. Instead of the intercept, we therefore resorted to the voltammetric response, $I_{p,\infty}$, obtained in a high volume-to-surface ratio cell for the same analyte concentration, $C^0_{N\text{-}AP}$, and therefore the same value of Γ^0_E. The value of V_{eff}/S was then derived from (see eqs 9 and 13)

$$\frac{I_{p,\infty}}{\text{slope}_{\text{thin-layer}}} = \frac{\delta}{D}\frac{V_{\text{eff}}}{S}$$

where $\text{slope}_{\text{thin-layer}}$ is the slope of the diagrams in Figure 10b′. It follows that $(V_{eff}/S)_{\text{thin-layer}} = 43 \pm 20$ μm, consistent with independent estimates leading to a value of ~60 μm (see Experimental Section).[70]

(c) As indicated in section 1.3, precipitating Ag^0 from the reaction of P with Ag^+, and recording its oxidation cyclic voltammogram as function of time, should in principle lead to a further improvement of the detection limit. The results of such experiments, carried with the same enzyme-labeled recognition system as in the preceding experiments are summarized in Figure 11. Two points are worth noting. One is that in the 10^2–10^5 fM N-AP concentration range, the current is not proportional to $C^0_{N\text{-}AP}$ contrary to what is expected from the Henry law relating Γ^0_E to $C^0_{N\text{-}AP}$ in the low N-AP concentration

(70) The slow decomposition of 2,6-DCPAP mentioned in section 2.1 (Figure 4) does not affect these results by more than a factor of 20% in the case of the droplet or 5% in the case of thin-layer cell.

range, a behavior that is indeed observed in all our experiments (see Figure 8). The same type abnormal behavior appears in the experiments, dealing with DNA hybridization, presented for the introduction of the method,[51] thus revealing the existence of an artifact in the relationship between the production of P and its translation as an Ag^0 precipitate. As second worrying observation is that there was no detectable signal for a N-AP concentrations below 100 fM. These observations, and similar ones that can be made with other precipitation techniques,[37,52] shed some doubts about their reliability.

3. Discussion of the Analytical Performances. Having tested the applicability of the theoretical relationships established in section 1, we may now use them to estimate the analytical performances of the approaches that we have envisaged, namely, steady state chronoamperometry; immediate cyclic voltammetry of the electroactive product generated under steady state conditions in a conventional cell; and delayed cyclic voltammetry of the electroactive product generated under steady state conditions in a small volume-to-surface area ratio, which allow its building up with time.

In all three cases, looking for the smallest detectable concentration of the analyte, $C^0_{\text{N-AP}}$, and, accordingly, to the smallest surface concentration of the recognized analyte Γ^0_E implies that the enzyme kinetics controls the current response and that the system lies in the linear portion of the current density: $C^0_{\text{N-AP}}$ or Γ^0_E-$C^0_{\text{N-AP}}$ curves, where: I or $I_p \propto k_2\Gamma^0_E$. It should be borne in mind that comparing the analytical performances of several heterogeneous bioaffinity assay methods implies comparing the lowest detectable surface concentration of the label that has been specifically immobilized on the solid phase, Γ^0_{label}, and not directly the lowest concentration, C^0_{analyte}, that can be detected in the incubation solution. Indeed, in the Henry region of the recognition isotherm (eq 14), the proportionality between Γ^0_{label} and C^0_{analyte} depends on the recognition binding constant and the label maximal coverage, according to:

$$\Gamma^0_{\text{label}} = \Gamma^0_{\text{label,max}} K_b C^0_{\text{analyte}} \tag{15}$$

and so for the proportionality between the current and C^0_{analyte}. For the same performance in terms of Γ^0_{label}, the performance in terms of C^0_{analyte} will be the better the larger the recognition binding constant is.

3.1. Simple Steady-State Chronoamperometry in Conventional Cells. Under these conditions, and assuming that the lowest detectable current response corresponds to 3 times the standard deviation of the blank current response, the detection limit of the label coverage, $\Gamma^0_{\text{label,min}}$, is then given by:

$$\Gamma^0_{\text{label,min}} = 3 \times \frac{\Delta I}{2Fk_2} \tag{16}$$

A key-factor of the analytical performance is thus the enzyme turnover. The other factor, ΔI, is the uncertainty on the measurement of the blank current density. From repeated experiments, a reasonable estimate is $\Delta I = 20$ nA/cm^2. Since, $k_2 = 1500$ s^{-1}, $\Gamma^0_{\text{label,min}} = 0.2$ fmol cm^{-2}, a performance that compares favorably with advanced fluorescence techniques (2 fluorophores/μm^2, i.e. 0.3 fmol/cm^2)[71] or nanoparticle-amplified surface-plasmon resonance (8×10^8 molecules/cm^2, that is, 1.3 fmol/cm^2).[72] Compared with other electrochemically detectable enzyme labels, especially redox enzyme labels (Scheme 1a) for which a relationship equivalent to eq 16 applies,[73] the N-AP label leads to a lower detectable enzyme label surface concentration because its turnover number for 2,6-DCPAPP (1500 s^{-1}) is higher than the turnover measured for redox enzyme labels such as horseradish peroxidase (280 s^{-1}) in the presence of the $[Os(bpy)_2pyCl]^{2+/+}$ mediator,[63] or as glucose oxidase toward its glucose substrate (600 s^{-1})[74] or biotinylated diaphorase toward its NADH substrate (700 s^{-1}).[73] As just recalled, in the case of redox enzyme labels the current response is entirely governed by the enzyme kinetics with no dependence upon the kinetics of mass transport. This is the reason that the sensitivity enhancement upon downscaling from a macroelectrode to an ultramicroelectrode reported in references 75, 76, and 77 seems puzzling.

As regards the lowest detectable concentration of the target analyte in solution we find, dealing with the avidin–biotin recognition, by application of eq 15 (with $\Gamma^0_{\text{label,max}} = 1500$ fmol cm^{-2} and $K_b = 5 \times 10^7$ M^{-1}, see section 2.2) a detection limit of the order of 2 pM. A concentration of 2 pM was indeed experimentally detected (see Figures 6 and 8).

3.2. Cyclic Voltammetry in High Volume-to-Surface Ratio Cells. Using cyclic voltammetry to detect the electroactive product of the enzymatic reaction, instead of the steady state chronoamperometry, allows an increase of the sensivity, that is, the ratio between the current response and the surface concentration or the incubation concentration of the labeled analyte (we note incidentally that this enhancement does not apply to redox enzyme labels involving a redox-mediated catalytic response). As seen in Figure 8, a typical value for this enhancement is a factor of 5. The average blank voltammetric current response can thus be determined with an improved precision. This is true if the uncertainty on this determination remains of the same order as in chronoamperometry. This is indeed the case, since an absolute uncertainty of $\Delta I = 25$ nA/cm^2 was found from the average cyclic voltammetric current recorded in a 1 mM 2,6-DCPAP (scan rate: 0.1 V/s), which is very close to the chronoamperometry value. Therefore the detection limit is expected to reach $\Gamma^0_{\text{label,min}} = 40$ amol cm^{-2} and $C^0_{\text{analyte,min}} = 0.4$ pM, with the avidin–biotin recognition system.

3.3. Accumulated Cyclic Voltammetry in Small Volume-to-Surface Ratio Cells. Product accumulation monitored by cyclic voltammetry, in small volume-to-surface ratio cells, is expected to result in further improvements. That this is indeed the case is seen in Figures 8 and 10, the detection limits being summarized in Table 1.

With the thinnest cell arrangement, after 1-hour reaction time, a value of $\Gamma^0_{\text{label,min}}$ as low as 0.2 amol/cm^2 could be reached, corresponding to a value of $C^0_{\text{analyte,min}} = 2$ fM for the avidin–biotin recognition system. These values compare favorably with those achieved by the most performing current techniques.

For example, with an AP label and the PAPP substrate, a detection limit of 54 fM of mouse IgG was found[27] with a

(71) Lehr, H.-P.; Reimann, M.; Brandenburg, A.; Sulz, G.; Klapproth, H. *Anal. Chem.* **2003**, *75*, 2414–20.
(72) He, L.; Musick, M. D.; Nicewarner, S. R.; Salinas, F. G.; Benkovic, S. J.; Natan, M. J.; Keating, C. D. *J. Am. Chem. Soc.* **2000**, *122*, 9071–7.
(73) Limoges, B.; Marchal, D.; Mavré, F.; Savéant, J.-M. *J. Am. Chem. Soc.* **2006**, *128*, 2084–92.
(74) Bourdillon, C.; Demaille, C.; Guéris, J.; Moiroux, J.; Savéant, J.-M. *J. Am. Chem. Soc.* **1993**, *115*, 12264–9.
(75) Zhang, Y.; Pothukuchy, A.; Shin, W.; Kim, Y.; Heller, A. *Anal. Chem.* **2004**, *76*, 4093–7.
(76) Zhang, Y.; Kim, H. H.; Heller, A. *Anal. Chem.* **2003**, *75*, 3267–9.
(77) Xie, H.; Zhang, C.; Gao, Z. *Anal. Chem.* **2004**, *76*, 1611–7.

Table 1. Detection Limits in Terms of Surface Concentration of the Enzyme Label and Solution Concentration of the Labeled Analyte for the Avidin–Biotin Recognition System

method	$\Gamma^0_{label,min}$ (amol cm^{-2})	$C^0_{analyte,min}$ (fM)
steady-state chronoamperometry in a standard cell ($V/S >> 10$ cm)	200	2000
immediate cyclic voltammetry[a] in a standard cell ($V/S >> 10$ cm)	40	400
cyclic voltammetric[a] detection after accumulation in small volume-to-surface ratio cells:		
droplet ($V/S = 0.25$ cm) with 1 h accumulation	13	130
thin-layer ($V_{eff}/S = 0.0043$ cm) with 20 min accumulation	0.5	5
thin-layer ($V_{eff}/S = 0.0043$ cm) with 1 h accumulation	0.2	2

[a] Scan rate: 0.1 V/s.

sandwich-type immunoassay performed in a self-contained microelectrochemical cell using cyclic voltammetry (50 μm diameter $\times$ 8 μm deep cavity with individually addressable electrodes, and a *V/S* ratio of 0.1 cm during the enzyme reaction). This result is consistent with our 130 fM N-AP detection limit obtained by cyclic voltammetry in a droplet ($V/S = 0.25$ cm), if we assume that the $\Gamma^0_{label}/C^0_{analyte}$ ratio is of the same order in both cases. The miniaturization of the electrochemical cell achieved in this study allows the detection of lower absolute amount of analyte. However, it does not provide per se any improvement of the detection limit. This is rather governed by the *V/S* parameter. Its further decrease to a value of 45 μm thus allows the detection of an analyte concentration as low as 2 fM. Although less simple to implement, it is worth noting that similar low *V/S* value can be reached in a microfluidic channel incorporating electrochemical detection.[78,79]

The detection limits achieved in the present work also compare well with the most sensitive labeling techniques developed so far, such as for example, silver-enhanced gold nanoparticle-label which were detected with an image analyzer at a surface concentration as low as 0.0025 nanoparticle-label/μm^2, that is, 0.5 amol/cm^2.[80–82] The femtomolar detection limit of our simple approach compare also favorably with sophisticated highly sensitive bioaffinity assays based on electrogenerated chemiluminescent (ECL) detection of DNA hybridization, with which a 1 fM concentration of a short oligonucleotide target could be detected.[83] To reach such a low concentration, the method takes advantage of polystyrene microbead labels loaded with a large amount of $[Ru(bpy)_3]^{2+}$ ($\sim 7.5 \times 10^9$ molecules per bead) which, following the binding event, was released in an acetonitrile solution for ECL measurement. Another approach based on the encapsulation of a large amount of a fluorophore within a silica nanoparticle label led to a detection limit of 0.8 fM for a 27-base length oligonucleotide.[84] In these two cases, the $\Gamma^0_{label}/C^0_{analyte}$ ratio is most probably not very different from our case,[85] indicating that our approach can potentially reach similar, if not better, analytical performances in DNA hybridization assays.

En route toward a further decrease of the cell thickness aiming at a further improvement of the detection limit, it is tempting to embark on a product precipitation strategy, which is indeed equivalent in principle to a decrease of the cell thickness. However, as seen in section 2.4, these approaches lack reliability.

Concluding Remarks

The theory of enzyme-amplified bioaffinity electrodes with electrochemical product detection has been established for several modes of detection. In the steady state chronoamperometric mode, product detection consists in measuring the steady-state current after imposition of a potential to the electrode sufficiently positive for the product to be immediately oxidized, preventing its diffusion toward the solution. The theoretical relationships that then link the electrochemical current response to the amount of recognized labeled target analyte on the surface are governed by two normalized parameters that measure the Michaelis–Menten competition in the enzyme, on the one hand, and the competition between the enzymatic kinetics and the diffusion of the substrate, on the other. The electrochemical response is eventually related to the labeled target analyte concentration in solution through the recognition isotherm. Application of this relationship offers a way to determine its characteristics, maximum coverage, and recognition binding constant. Guided by the theoretical relationships, careful analysis of the experimental data allows elimination of the interference of substrate diffusion so as to derive a true recognition isotherm.

Further theoretical relationships have been derived for cyclic voltammetric detection of the electroactive product generated under steady-state diffusion-natural convection conditions, in standard cells or by accumulation of the enzyme–product in cells of large surface/volume ratios. The same two normalized parameters govern the peak current density. This is amplified as compared to the chronoamperometric response by a factor that increases with the scan rate. In cells of small volume/surface ratios, the peak current increases linearly with time, which provides an additional source of amplification. Although less sensitive, the voltammetric detection of the enzyme-generated product without accumulation has the advantage of being well-suited to electrochemical detection systems involving array-based bioaffinity electrodes for multianalyte affinity assays.[5]

The avidin–biotin recognition process in a system that involves alkaline phosphatase as enzyme label and 4-amino-2,6-dichlorophenyl phosphate as substrate, generating 4-amino-2,6-dichlorophenol as electrochemically active product has proved to be particularly pertinent for testing the theory. The agreement between theoretical predictions and experiment was found excellent in all detection regimes.

(78) Rossier, J. S.; Girault, H. H. *Lab on a Chip* **2001**, *1*, 153–7.
(79) Ronkainen, N. J.; Thomas, J. H.; Halsall, H. B.; Heineman, W. R. *Trends Anal. Chem.* **2002**, *21*, 213–25.
(80) Taton, T. A.; Mirkin, C. A.; Letsinger, R. L. *Science* **2000**, *289*, 1757–60.
(81) Bao, Y. P.; Wei, T. F.; Lefebvre, P. A.; An, H.; He, L.; Kunkel, G. T.; Müller, U. R. *Anal. Chem.* **2006**, *78*, 2055–9.
(82) Storhoff, J. J.; Marla, S. S.; Bao, P.; Hagenow, S.; Mehta, H.; Lucas, A.; Garimella, V.; Patno, T.; Buckingham, W.; Cork, W.; Müller, U. R. *Biosens. Bioelectron.* **2004**, *19*, 875–83.
(83) Miao, W.; Bard, A. J. *Anal. Chem.* **2004**, *76*, 5379–86.
(84) Zhao, X.; Tapec-Dytioco, R.; Tan, W. *J. Am. Chem. Soc.* **2003**, *125*, 11474–5.
(85) Affinity binding constants of 10^7-10^9 M^{-1}, with a maximal binding coverage of few pmol/cm^2, have been found for heterogeneous DNA hybridization of short ($\sim$20–25 bases) complementary oligonucleotide sequences on solid surface.[71,72,86–88]
(86) Okahata, Y.; Kawase, M.; Niikura, K.; Ohtake, F.; Furusawa, H.; Ebara, Y. *Anal. Chem.* **1998**, *70*, 1288–96.
(87) Niemeyer, C. M.; Burger, W.; Hoedemakers, R. M. J. *Bioconjugate Chem.* **1998**, *9*, 168–75.
(88) Fang, S.; Lee, H. J.; Wark, A. W.; Corn, R. M. *J. Am. Chem. Soc.* **2006**, *128*, 14044–6.

Scheme 6. Synthesis of Zwitterionic Form of 4-Amino-2,6-dichloro-phenyl Phosphate [a]

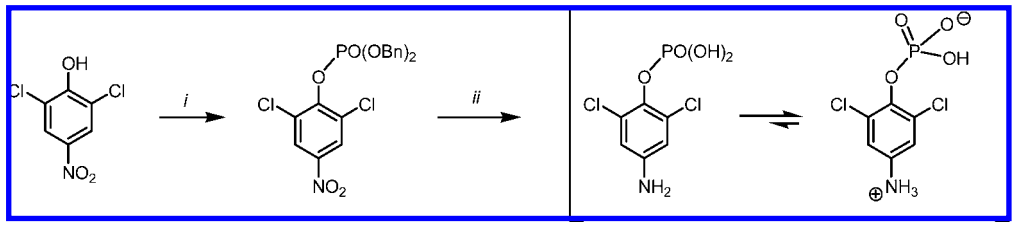

[a] (i) CCl_4, $HPO(OBn)_2$, NEt_3, CH_3CN; (ii) H_2, 10% $Pd/CaCO_3$, CH_3OH.

The enzyme–product, 2,6-DCPAP, has the further advantage to be reversible even at an electrode partially blocked with protein layers. Such a well-defined electrochemical reversibility is particularly attractive for improving the sensitivity by enzyme[62,89] or electrochemical[28,35] recycling of the enzyme-generated redox product as discussed in the following companion paper.

Taking the various theoretical factors into account, the analytical performances could finally be discussed in a systematic way so as to rationally and realistically estimate the detection limits for all regimes. The values thus reached are summarized in Table 1. The lowest value was achieved with cyclic voltammetric detection after accumulation in a thin-layer cell of 40 μm thickness. Then a value of 0.2 amol/cm^2 is reached after 1-hour accumulation, corresponding to 2 fM of target analyte in solution for the avidin–biotin system.

These performances compare favorably not only with those of other electrochemical techniques but also with those of sophisticated amplification techniques coupled with silver-enhanced gold nanoparticle-label detected with an image analyzer[80–82] or with fluorescent-based detection of nanoparticle-label loaded with a large amount of fluorophores.[84,90]

Another clear advantage compared with other high-sensitivity methods is the linearity of calibration curve (slope 1 in log–log scale) over several orders of magnitude, providing a sound basis for precise and sensitive quantitation.

Finally, the analytical performances of the method can also be improved by multiplying the number of enzymes per conjugate. In the present study, there is only one AP label per avidin, but it is possible to replace it by large carrier labels such as carbon nanotubes or microparticles loaded with numerous enzymes. It has for example been shown that several thousands of AP can be attached to a carbon nanotube.[91] Several orders of magnitude improvement in sensitivity could thus be obtained by combining this strategy with our electrochemical approach. Likewise combination with a second enzyme should also lead to further improvements as demonstrated in a preliminary communication.[89]

Experimental Section

Reagents. *p*-Aminophenol (Prolabo), 2,6-dichloro-4-aminophenol, *p*-nitrophenyl phosphate (Sigma), bovine serum albumine (BSA) (Sigma), chrompure biotinylated rabbit IgG (Pierce), and neutravidin-conjugated alkaline phosphatase (Pierce, according to the supplier one phosphatase is coupled to one molecule of neutravidin) were used as received. The $[Os(bpy)_2pyCl]PF_6$ was obtained as previously described.[63] A phosphate buffer saline (PBS) of pH 7.4 was prepared from 4.3 mM NaH_2PO_4, 15.1 mM Na_2HPO_4, and 50 mM NaCl. A 0.1 M Tris buffer (TB) of pH 9.0 containing $MgCl_2$ was prepared from 5.54 mM Trizma base (Sigma) and 3 mM Trizma, HCl (Sigma), and 1 mM $MgCl_2{\cdot}6H_2O$. All aqueous solutions were prepared with water purified by a Milli-Q water purification system from Millipore. Concentrated stock solutions of 2,6-DCPAP were prepared in absolute ethanol. Diluted standard solutions of 2,6-DCPAP were prepared in TB and used immediately.

Synthesis of 4-Amino-2,6-dichlorophenyl Phosphate. The 4-amino-2,6-dichlorophenylphosphate was prepared in two steps from the commercially available 2,6-dichloro-4-nitrophenol, as depicted in Scheme 6. During hydrogenation, both the protecting benzyl groups were removed and the nitro group was reduced to the free amine. Taking advantage of the low solubility of the zwitterion, a pure monoester phosphate was finally obtained.

(4-Amino-2,6-dichlorophenyl)-dibenzyl Phosphate Ester. The dibenzyl phosphate ester was prepared according to a slightly modified procedure of the general method given by Silverberg.[55] The starting compound 2,6-DCPAP (1.0 g, 4.81 mmol) was dissolved in anhydrous acetonitrile (20 mL) under argon atmosphere. At −10 °C, tetrachloromethane (2.32 mL, 24.04 mmol), *N*,*N*-diisopropylamine (1.76 mL, 10.10 mmol) and *N*,*N*-dimethylaminopyridine (59 mg, 0.48 mmol) were added successively under stirring. Then dibenzyl phosphite (1.70 mL, 7.69 mmol) was added dropwise. After 2 h, the reaction was complete as determined by thin-layer chromatography. Then, 0.5 M aqueous KH_2PO_4 (20 mL) was added and the reaction mixture was brought to room temperature. The mixture was extracted three times with ethyl acetate. The combined organic phase was washed successively with water and brine, dried over magnesium sulfate, and concentrated in vacuo. The crude product (2.57 g) was purified by recrystallization from ethanol (40–50 mL). The pure dibenzyl phosphate ester was collected as uncolored needles in 71% yield (1.60 g, 3.42 mmol). ^{1}H NMR ($CDCl_3$, 250 MHz) δ/ppm 8.12 (s, 2H, aromatic), 7.27 (s, 10H, phenyl), 5.16 (d, 4H, J = 8.4 Hz, P-CH_2). ^{31}P NMR ($CDCl_3$, 250 MHz) δ/ppm −7.74. ^{13}C NMR ($CDCl_3$, 250 MHz) δ/ppm 149.23, 144.43, 135.04, 134.93, 129.56, 128.88 (CH), 128.69 (CH), 128.08 (CH), 124.43 (CH), 70.94 (CH_2), 70.85 (CH_2). Anal. Calcd for $C_{20}H_{16}Cl_2NO_6P$: C, 51.30; H, 3.44; N, 2.99. Found: C, 51.26; H, 3.53; N, 2.89.

2,6-Dichloro-4-aminophenyl Phosphate. A solution of (4-amino-2,6-dichlorophenyl)-dibenzyl phosphate ester (0.96 g, 2.05 mmol) in methanol (140 mL) was ultrasonicated for 10 min and purged with argon. Ten-percent palladium on calcium carbonate (1 g) was added and 1 bar of hydrogen pressure was applied for 12 h under vigorous stirring at room temperature. The reaction mixture was purged with argon and 1% aqueous ammonia (20 mL) was added to completely dissolve the product. After filtration over cellite (2 washings with a solution of 1% ammonia in 5 mL water/10 mL methanol mixture) the filtrate was titrated with 0.5 M sulfuric acid until pH 4. The mixture was concentrated under vacuum until total evaporation of methanol and then kept for 1 h at 0 °C. The precipitate was filtered off, rinsed two times with cold water, and dried at 50 °C under vacuum for 3 h affording 322 mg colorless needles of the zwitterionic form of 4-amino-2,6-dichlorophenyl phosphate (1.36 mmol, 67% yield). ^{1}H NMR (D_2O, 250 MHz)

(89) Limoges, B.; Marchal, D.; Mavré, F.; Savéant, J.-M. *J. Am. Chem. Soc.* **2006**, *128*, 6014–5.
(90) Matsuya, T.; Tashiro, S.; Hoshino, N.; Shibata, N.; Nagasaki, Y.; Kataoka, K. *Anal. Chem.* **2003**, *75*, 6124–32.
(91) Wang, J.; Liu, G.; Jan, M. R. *J. Am. Chem. Soc.* **2004**, *126*, 3010–1.

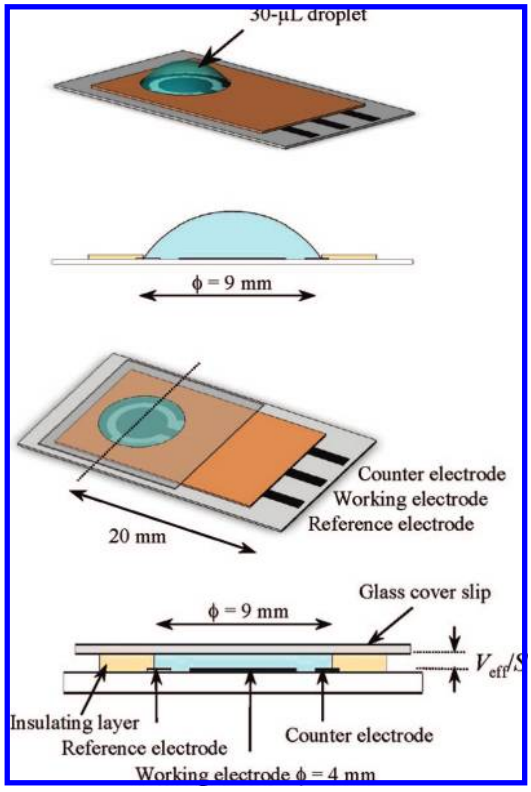

Figure 12. Droplet and thin-layer small volume-to-surface ratio cells.

δ/ppm 6.79 (s). ^{1}H NMR (CD_3OD, 250 MHz) δ/ppm 6.64 (s). ^{1}H NMR (pyridin-d5, 250 MHz) δ/ppm 6.89 (s). ^{31}P NMR (D_2O, 250 MHz) δ/ppm 0.42 (s). ^{31}P NMR (CD_3OD, 250 MHz) δ/ppm −3.84 (s). ^{31}P NMR (pyridine-d5, 250 MHz) δ/ppm −2.50 (s). MS-ES (TOF^+), *m/z* (relative intensity, fragment): 514.9 (50%, M+M-1, dimer), 255.9 (100%, M-1 with ^{35}Cl,^{35}Cl), 257.9 (55%, M-1 with ^{35}Cl,^{37}Cl), 259.9 (7%, M-1 with ^{37}Cl,^{37}Cl), 222 (70%, [M - Cl]). Anal. Calcd for $C_6H_6Cl_2NO_4P$: C, 27.93; H, 2.34; N, 5.43; P, 12.01. Found: C, 29.59; H, 2.77; N, 5.62; P, 11.70.

Electrochemical Experiments. An AUTOLAB potentiostat (Ecochemie) interfaced to a PC computer (GPES software) was used for cyclic voltammetry and chronoamperometry. For the experiments performed in a large volume of substrate solution (*V/S* >> 10), small screen-printed carbon electrodes (1.5-mm diameter) were used as disposable working electrodes. They were prepared from a commercial carbon-based ink (Electrodag PF-407A, Acheson Colloid) printed on a sheet of transparency film (3M). A manual screen-printer (Circuit Imprimé Français, Bagneux, France) equipped with a screen-stencil of 77 threads cm^{-1} was used. In a few experiments a freshly polished glassy carbon electrode (3-mm diameter) was used as working electrode. A classical water-jacketed electrochemical cell (maintained at 20 ± 0.5 °C) equipped with a saturated calomel reference electrode (SCE) and a platinum counter electrode was used. For the experiments carried out with a low *V/S* cell configuration, electrochemical microcells (Andcare) integrating three screen-printed electrodes on a planar sheet (i.e., two carbon electrodes as the working and counter electrodes, and a Ag/AgCl pseudoreference) were used (Figure 12). In this configuration the working electrode area was 0.125 cm^2 and the overall electrodes were delimited by a circular thick insulating layer (9-mm diameter) allowing the definition of an electrochemical microcell of a few tens of microliters. It is worth noting that in the case of standard ELISA performed in classical wells of a microtiter plate, the *V/S* is of ~0.2 cm, which is not far from the format of our droplet deposited in the electrochemical microcell.

The voltammetric curves presented in this work were systematically referred to SCE. The diffusion coefficient of 2,6-DCPAP was determined in cyclic voltammetry at 20 °C and using a glassy carbon electrode. A value of 4×10^{-6} cm^2 s^{-1} was found. To check the electron transfer rate through a protein film adsorbed on the electrode, screen-printed carbon electrodes and glassy carbon electrodes were coated with a monolayer of BSA by dipping the electrode in a 0.1 wt % BSA solution for 15 min.

Preparation of b-IgG-Modified Carbon Electrodes and Affinity Binding of N-AP. Unless otherwise stated, all experiments were performed at room temperature. Drops of 0.5 mg mL^{-1} biotinylated rabbit IgG in PBS were locally deposited on the sensing area of the working screen-printed carbon electrodes (drops of 1.5 µL in the case of the 0.0176 cm^2 electrode and 10 µL in the case of the 0.125 cm^2 Andcare's working electrode were used) and incubated for 2 h in a water-saturated atmosphere. After thorough washing with PBS, b-IgG-modified carbon electrodes were dipped in PBS containing 0.1 wt % BSA for 20 min and next in a solution of N-AP diluted in TB (0.5 mL for the 0.0176 cm^2 screen-printed carbon electrodes and 5 mL for the Andcare electrodes) for at least 12 h (the N-AP concentration was ranged from 5×10^{-15} to 2×10^{-7} M). For control experiments, the first layer of b-IgG was replaced by BSA. Once prepared, enzyme electrodes were rinsed and stored in PBS at 4 °C until used.

For experiments involving accumulation of the enzyme-generated product in a low volume-to-surface cell two configurations have been used (Figure 12). Both were based on planar Andcare screen-printed electrochemical cell. The first one consists of a deposit of a small droplet of 30 µL of enzyme–substrate solution (1 mM 2,6-DCPAPP in TB) over the screen-printed electrochemical cell (Figure 12) and monitoring the accumulated product periodically, from a few seconds to 1 h, by cyclic voltammetry. During the enzyme reaction, the electrochemical cell was in a chamber saturated with humidity to minimize evaporation of the droplet. The second configuration consists of confining 4 µL of the enzyme–substrate solution (1 mM 2,6-DCPAPP in TB) between a planar screen-printed electrochemical cell and a glass coverslip for microscope slide (Figure 12) and, as for the droplet configuration, monitoring the accumulated product by cyclic voltammetry. The thickness of thin-layer cell was indirectly determined from the cyclic voltammetry of a solution of $[Os(bpy)_2pyCl]^+$ (0.1 mM). Upon rising the scan rate, the transition in voltammetry from a thin-layer to a semi-infinite diffusion layer ($l = 4 \times 0.446(DRT/Fv)^{1/2}$) allows us to calculate a film thickness of 60 µm (using for the $[Os(bpy)_2pyCl]^+$ a diffusion coefficient of 4.5×10^{-6} cm^2 s^{-1}). This measured value is in agreement with the film thickness of $l = 63$ µm that can be calculated from the geometrical dimensions of the electrochemical microcell (9-mm diameter) and the 4 µL of liquid deposited within the cell.

For experiments involving the reductive precipitation of silver induced by the enzyme-generated product, the N-AP/b-IgG-modified screen-printed carbon electrodes (1.5-mm diameter), prepared as above with different N-AP coverage, were immersed in a Tris buffer of pH 9 (adjusted with H_2SO_4) containing 2 mM $MgSO_4$, 1 mM PAPP, and 2 mM $AgNO_3$ for 30 min in a black room.[51] After a thorough washing, the N-AP modified electrodes were scanned by anodic stripping voltammetry in a 2 N H_2SO_4.

Electrochemical Characterization of 2,6-DCPAPP. A mass (1.27 mg) of the 2,6-DCPAPP powder was dissolved in water (57.72 µL). A 50 µL portion of this solution was introduced in the electrochemical cell containing 2.45 mL of TB and 5 µL of a 10.5 µM N-AP solution. After 5 min of enzyme reaction, a cyclic voltammogram was recorded showing the typical reversible wave of 2,6-DCPAP. Considering that all of the 2,6-DCPAPP was hydrolyzed into 2,6-DCPAP within 5 min, it was possible to deduce from the magnitude of the reversible peak currents and the diffusion coefficient of 2,6-DCPAP the initial amount of 2,6-DCPAPP added into the cell. Taking in account dilution and mass of powder dissolved, we thus calculated an apparent molecular weight of 329.5 g mol^{-1} for 2,6-DCPAPP.

Homogeneous Kinetics of N-AP with 2,6-DCPAPP as Substrate. The homogeneous kinetics of the reaction of N-AP with 2,6-DCPAPP were determined both spectrophotometrically and electrochemically. For spectrophotometric measurements, a UV–visible Hewlett-Packard 8452 diode array spectrophotometer interfaced with a PC computer was used and the temperature of the standard quartz cell (1-cm path length) was maintained at 20 °C. Steady-state kinetics were studied by following at 324 nm the initial rate of 2,6-DCPAP production ($\epsilon_{324nm} = 3525\ M^{-1}\ cm^{-1}$) as a function of the substrate concentration (ranging from 10 to 1500 μM). The reactions were initiated by addition of the 2,6-DCPAPP substrate to a solution of N-AP (5×10^{-11} M) in TB (pH 9.0) containing 0.1 wt % BSA. The reciprocal plot of the dependence of the initial rate on the initial concentration of 2,6-DCPAPP was fitted to a Lineweaver–Burke plot, and values of $k_2 = 1837 \pm 73\ s^{-1}$ and $K_M = 48 \pm 3\ \mu M$ were determined.

For the electrochemical characterization of the homogeneous kinetics of N-AP, amperometry at controlled potential was used. The amperometric responses were recorded at a glassy carbon electrode (polarized at 0.25 V vs SCE) immersed in a solution containing 0.05 nM N-AP in TB, 0.1 wt% BSA, and different concentrations of 2,6-DCPAPP (ranging from 30 to 500 μM) that were injected immediately after the current was stabilized. The initial linear increases of the current responses as a function of the substrate concentration were used to calculate the initial rates of 2,6-DCPAP produced in the bulk of the solution. From the fitting of the data to a Lineweaver–Burke plot, values of $k_2 = 1073 \pm 163\ s^{-1}$ and $K_M = 67 \pm 31\ \mu M$ were obtained. The N-AP kinetics was also determined amperometrically at a lower pH of 6.5 (MES buffer containing 0.1 wt % BSA and 1 mM $MgCl_2$). Under these conditions, values of $k_2 = 45 \pm 2\ s^{-1}$ and $K_M = 20 \pm 4\ \mu M$ were found.

Determination of the Enzyme Coverage from Depletion of N-AP Contained in a Droplet Deposited on the b-IgG-Coated Electrode. The enzyme coverage was independently determined using the droplet depletion method previously developed by us for horseradish peroxidase and extended here for AP.[63] The following procedure was applied. Drops of 1 μL containing 0.5 mg mL^{-1} b-IgG in TB were deposited on the active surface of a series of screen-printed carbon electrodes and incubated for 2 h in a water-saturated atmosphere at 4 °C. The electrodes were then rinsed with TB and dipped for 15 min in 2 mL TB containing 0.1 wt % BSA. After another washing with TB, drops of 1.5 μL of 0.05 μM N-AP in TB containing 0.1 wt % BSA were deposited on the surface of modified screen-printed carbon electrodes and then further incubated for 2 h in a water-saturated atmosphere at 4 °C. Next, each extremity of the electrodes with their droplet over the surface were immersed and rinsed for 5–10 min in a vial filled with 2 mL TB containing 0.1 wt % BSA. The activity of N-AP contained into the vial was then measured spectrophotometrically by monitoring the increase of absorbance at 396 nm after the addition of 20 μL of 50 mM *p*-nitrophenyl phosphate substrate in TB. The unknown diluted N-AP concentration was finally determined from a standard calibration plot of N-AP ranging from 12.5 to 50 pM. From the determined concentration, the amount of N-AP immobilized on the electrode was indirectly inferred. An average N-AP coverage value of 1.5 ± 0.3 pmol cm^{-2}, corrected from nonspecific adsorption, was finally estimated. This result is relevant to the theoretical value that can be roughly estimated from the protein sizes of a packed monolayer of N-AP (i.e., 1.7 pmol cm^{-2} for a saturated monolayer).

JA7102845